

© 2012 Cathy Chu

ENGINEERING MATRIX PROPERTIES FOR STEM CELL CULTURE AND GENE
DELIVERY

BY
CATHY CHU

DISSERTATION

Submitted in partial fulfillment of the requirements
for the degree of Doctor of Philosophy in Chemical Engineering
in the Graduate College of the
University of Illinois at Urbana-Champaign, 2012

Urbana, Illinois

Doctoral Committee:

Assistant Professor Hyunjoon Kong, Chair
Assistant Professor Mary L. Kraft
Professor Daniel W. Pack
Associate Professor Marie-Claude Hofmann

ABSTRACT

Tissue engineering aims to regenerate lost or damaged tissues and frequently combines therapeutic cells, biomaterial scaffolds, and therapeutic molecules in efforts to do so. One of the primary considerations in such therapies is to orchestrate the interactions between these components to regulate the desired cellular responses. This thesis focuses on tuning the proliferation of and exogenous protein expression from precursor cells, multipotent stem cells, and pluripotent stem cells with the mechanical and chemical properties of hydrogel-based synthetic extracellular matrices (ECMs). First, a synthetic stem cell niche with controlled stiffness and density of cell adhesion peptides was developed for spermatogonial stem cell (SSC) culture (Chapter 2). The synthetic stem cell niche allowed for the growth of SSCs in both two-dimensional (2D) and three-dimensional (3D) cultures, and the proliferation of SSCs was influenced by the density of cell adhesion ligands but not by substrate stiffness. Separately, the effects of substrate stiffness on non-viral gene delivery were evaluated for stem and precursor cells commonly used in tissue engineering or frequently present at gene delivery sites (Chapter 3). The cellular uptake and expression of non-viral genes for fibroblasts, bone marrow stromal cells (BMSCs), and myoblasts were regulated by the stiffness of the synthetic ECM. Interestingly, the effects of matrix stiffness on non-viral gene delivery were dependent on cell type, likely due to differences in cellular sensitivity to matrix mechanics. Finally, the results from the first two sections were used to build an implantable microvascular stamp consisting of cells transfected with plasmid DNA encoding vascular endothelial growth factor (VEGF) and a hydrogel matrix with tunable stiffness and permeability (Chapter 4). Overall, the results from this thesis may be useful in understanding the role of the extracellular microenvironment in

tuning a variety of cellular activities. Furthermore, the information gained from these studies may be instrumental in the design and development of a novel biomaterial to significantly enhance the quality of tissue regeneration therapies.

To my family

ACKNOWLEDGEMENTS

First, I would like to thank my advisor, Professor Hyunjoon Kong for his guidance and support throughout the years. I would like to thank the entire Kong Research Group, especially John Schmidt for his insight, support, and encouragement. Thank you also to Dr. JaeHyun Jeong and Vincent Chan for collaborating on the microvascular stamp project as well as Dr. Richie Kohman for sharing his expertise in chemical synthesis. I would like to thank the Hofmann Research Group for their collaborative work on the spermatogonial stem cell project. Thank you to my committee members, Professor Mary Kraft, Professor Daniel Pack, and Professor Marie-Claude Hofmann.

I would like to thank all the people who have made my experience at the University of Illinois truly memorable. A special thanks to Illinois Women's Ultimate, especially Katie Shiro who reminds me to push every day. I would like to thank my roommate, Neera Jain, for her support and encouragement. Thank you to all the people I met during graduate school and all the friends I made along the way. Thank you to all my friends from undergrad for their support over the years. A special thank you to Keith Jordy for his unconditional support throughout all my endeavors.

Finally, I would like to thank my mom, my dad, and my brother, Kevin, for their endless love and support. Thank you for teaching me the value of hard work and for being a constant source of inspiration. Thank you for helping me become the person I am today, and thank you for all the opportunities you have given me without which none of this this would have been possible.

TABLE OF CONTENTS

LIST OF FIGURES	ix
CHAPTER 1: INTRODUCTION	1
1.1 Tissue engineering	1
1.1.1 Hydrogels in tissue engineering.....	1
1.1.1.1 Alginate.....	3
1.1.1.2 Poly(ethylene glycol).....	6
1.1.2 Stem cells in tissue engineering.....	6
1.2 Synthetic extracellular matrices.....	8
1.2.1 Effects of matrix stiffness on cell behavior	9
1.2.2 Effects of cell adhesion cues on cell behavior	10
1.3 Gene therapy	11
1.3.1 Delivery of therapeutic genes	12
1.3.2 Gene therapy in tissue engineering.....	13
1.4 Project overview	15
1.5 References.....	16
CHAPTER 2: THREE-DIMENSIONAL SYNTHETIC NICHE FOR SPERMATOGONIAL STEM CELL CULTURE	21
2.1 Introduction.....	21
2.2 Objective and scope	23
2.3 Materials and methods	24
2.3.1 Alginate modification	24
2.3.2 Cell line and cell culture	25
2.3.3 Two-dimensional cell culture on hydrogels.....	25
2.3.4 Three-dimensional cell culture in hydrogels.....	26
2.3.5 Analysis of stress fibers for 2D cultures	26
2.3.6 Cell proliferation assay for 2D cultures	27

2.3.7	Cell proliferation and viability assays for 3D cultures	27
2.3.8	Immunohistochemistry analysis for 3D cultures	28
2.3.9	Statistical analysis	28
2.4	Results	29
2.4.1	Effects of RGD peptide densities and hydrogel stiffness on cell proliferation in 2D cultures	29
2.4.2	Effects of RGD peptide densities on cell proliferation in 3D cultures	30
2.5	Discussion	32
2.6	References	35
2.7	Figures	38

CHAPTER 3: INTERPLAY OF CELL ADHESION MATRIX STIFFNESS AND CELL

TYPE FOR NON-VIRAL GENE DELIVERY	52
3.1 Introduction.....	52
3.2 Objective and scope	53
3.3 Materials and methods	54
3.3.1 Poly(ethylene glycol) diacrylate hydrogel preparation.....	54
3.3.2 Cell culture on hydrogels of varied stiffness	55
3.3.3 Analysis of cell proliferation	55
3.3.4 Delivery of pDNA encoding BMP-2 and evaluation of BMP-2 expression	56
3.3.5 Analysis of cellular uptake of fluorescently-labeled pDNA.....	57
3.3.6 Analysis of projected cell area and nuclear aspect ratio	58
3.3.7 Statistical analysis.....	59
3.4 Results.....	59
3.4.1 Characterization of poly(ethylene glycol) diacrylate hydrogels	59
3.4.2 Cellular uptake of pDNA encoding BMP-2 and resulting BMP-2 expression as mediated by matrix stiffness.....	60
3.4.3 Effect of matrix stiffness on cell proliferation.....	61
3.4.4 Effect of matrix stiffness on cellular morphology	61
3.5 Discussion.....	62
3.6 Conclusion	65

3.7 References.....	68
3.8 Figures.....	69
CHAPTER 4: MICROVASCULAR STAMP WITH GENETICALLY MODIFIED CELLS	
FOR REVASCULARIZATION THERAPIES	80
4.1 Introduction.....	80
4.2 Objective and scope	82
4.3 Materials and methods	83
4.3.1 Methacrylic alginate synthesis.....	83
4.3.2 Poly(ethylene glycol) diacrylate synthesis.....	83
4.3.3 Hydrogel formulation and analysis	84
4.3.4 Cell culture and transfection	85
4.3.5 Cell encapsulation in hydrogels	86
4.3.6 Cell encapsulation in microvascular stamps using SLA.....	86
4.3.7 Cell viability and VEGF secretion assays.....	87
4.3.8 Chorioallontic membrane-based angiogenesis assay	88
4.4 Results and discussion	88
4.4.1 Effects of pDNA dosage on gene expression and cell viability.....	88
4.4.2 Effects of polymer composition on hydrogel pore size and viability of encapsulated cells.....	89
4.4.3 Cell viability and VEGF secretion from microvascular stamps	90
4.4.4 Blood vessel formation from microvascular stamps in a CAM-based angiogenesis assay	91
4.5 Conclusion	92
4.6 References.....	93
4.7 Figures.....	95

LIST OF FIGURES

Figure 2.1	RGD-alginate synthesis	38
Figure 2.2	Alginate hydrogel formation.....	39
Figure 2.3	Effect of N_{RGD} on SSC actin stress fiber formation in 2D	40
Figure 2.4	Effect of N_{RGD} on SSC colony formation in 2D	41
Figure 2.5	Effect of N_{RGD} on SSC colony size in 2D	42
Figure 2.6	Effect of N_{RGD} on SSC cell number over time in 2D	43
Figure 2.7	Effects of N_{RGD} on proliferation rate of SSCs in 2D.....	44
Figure 2.8	Effects of substrate stiffness on SSC cell number over time in 2D	45
Figure 2.9	Effects of substrate stiffness on SSC proliferation	46
Figure 2.10	Effect of N_{RGD} on SSC colony formation in 3D	47
Figure 2.11	Effect of N_{RGD} on SSC colony size in 3D	48
Figure 2.12	Effect of N_{RGD} on cell viability in 3D	49
Figure 2.13	Effect of N_{RGD} on SSC proliferation in 3D	50
Figure 2.14	Immunocytochemistry analysis of SSC colonies in 3D.....	51
Figure 3.1	PEGDA Hydrogel characterization.....	69
Figure 3.2	Uptake of fluorescently-labeled pDNA	70
Figure 3.3	Quantification of cellular uptake of pDNA	71
Figure 3.4	Effects of substrate stiffness on absolute BMP-2 expression	72
Figure 3.5	Effects of substrate stiffness on cellular metabolic activity.....	73
Figure 3.6	Effects of substrate stiffness on normalized BMP-2 expression	74
Figure 3.7	Effects of substrate stiffness on BMP-2 expression from electroporation	75
Figure 3.8	Effects of substrate stiffness on cell proliferation.....	76
Figure 3.9	Analysis of cellular morphology.....	77
Figure 3.10	Effects of substrate stiffness on projected cell area	78
Figure 3.11	Effects of substrate stiffness on nuclear aspect ratio	79
Figure 4.1	“Living” microvascular stamp for patterning of functional neovessels.....	95

Figure 4.2	Synthesis of methacrylic alginate (MA)	96
Figure 4.3	Synthesis of poly(ethylene glycol) diacrylate (PEGDA).....	97
Figure 4.4	Stereolithography apparatus (SLA) for microvascular stamp fabrication	98
Figure 4.5	In-shell CAM angiogenesis assay	99
Figure 4.6	Effect of pDNA dose on VEGF expression.....	100
Figure 4.7	Effect of pDNA dose on cell viability	101
Figure 4.8	Hydrogel pore size	102
Figure 4.9	Cell viability following encapsulation in microvascular stamp.....	103
Figure 4.10	VEGF secretion from microvascular stamps	104
Figure 4.11	Cell viability in microvascular stamps.....	105
Figure 4.12	Blood vessel formation from microvascular stamps.....	106
Figure 4.13	Inflammatory response from microvascular stamp with high cell density	107

CHAPTER 1: INTRODUCTION

1.1 Tissue engineering

Tissue engineering is a field that combines engineering and life sciences principles with the goal of repairing or replacing lost or damaged tissues (Langer and Vacanti, 1993). Since the field emerged, several tissue engineering products have been commercialized, including artificial skin and cartilage (Khademhosseini et al, 2009). Biomaterials, cells, and therapeutic molecules are frequently used in concert to engineer new tissues or regenerate damaged tissues (Hirano and Mooney, 2004), and much research has been focused on developing biomaterials for use as tissue engineering scaffolds or synthetic cell niches (Griffith and Naughton, 2002; Ratner and Bryant, 2004; Lutolf and Hubbell, 2005). Furthermore, harvesting and engineering therapeutic cells along with the use of therapeutic molecules is critical to achieve the ultimate goal of engineering new tissues (Badylak and Nerem, 2010).

1.1.1 Hydrogels in tissue engineering

Hydrogels are viscoelastic materials formed from cross-linking hydrophilic polymers dissolved in aqueous media. These materials have been widely used for biological applications (Hoffman, 2002; Peppas et al, 2006). Due to structural similarities to the native extracellular matrix (ECM), hydrogels are well-suited for tissue engineering applications (Drury and Mooney, 2003). Hydrogels can be used as scaffolds to provide space for tissue regeneration and also as synthetic extracellular matrices to deliver cells and therapeutic molecules (Lee and Mooney, 2001). Hydrogels can be generally classified as naturally-derived polymers, which include collagen, hyaluronic acid, chitosan, and alginate, and synthetic polymers, which include poly(2-

hydroxyethylmethacrylate) (HEMA), poly(N-isopropylacrylamide) (PNIPAAm), and poly(ethylene glycol) (PEG).

Depending on their intended applications, hydrogels must present certain physical and biological properties. Physical properties include gel formation mechanisms, mechanical properties, and degradation behavior. Gel formation mechanisms are critical to consider when incorporating cells or molecules, as certain processing techniques can kill cells or denature molecules of interest (Schmidt et al, 2008). Implantable scaffolds must present the mechanical properties needed to withstand loads encountered in the body while supporting cell growth for tissue regeneration. For tissue engineering applications, it may be necessary to design degradable scaffolds to allow new tissue formation or to release therapeutic molecules of interest. Hydrogel scaffolds typically degrade through hydrolysis, enzymatic degradation, or dissolution. The porous structure of hydrogel scaffolds is also an important consideration, as it governs the diffusive behaviors of gases, nutrients, proteins, cells, and waste. While the non-toxic nature of hydrogels makes them suitable materials for biological applications, most hydrogel materials do not support cell adhesion, which is frequently necessary in tissue engineering. Collagen, which is a natural ECM protein, is a notable exception. Hydrogels also do not typically permit protein absorption due to their hydrophilic nature. Thus, covalent modifications are frequently used to couple cell adhesion proteins or therapeutic growth factors to hydrogels for tissue engineering applications (Lee and Mooney, 2001; Drury and Mooney, 2003).

Collagen is the most abundant protein in mammalian tissues and is one of the most widely used naturally-derived hydrogel materials. Collagen consists of three intertwined polypeptide chains which are held together with hydrogen bonds and covalent bonds. These

intertwined chains can self-aggregate to form fibers, which are the structural component in collagen hydrogels. Collagen hydrogels present many ideal biological properties for tissue engineering and are enzymatically degradable; however, collagen has limited physical properties. Chemical cross-linking with molecules such as glutaraldehyde and formaldehyde has been used to improve the physical strength of collagen hydrogels. Hyaluronic acid is a glycosaminoglycan found in the native ECM. Hyaluronic acid is a linear polysaccharide that can be covalently cross-linked with hydrazide derivatives to form hydrogels or combined with collagen to form composite hydrogels. Chitosan is a linear polysaccharide derived from chitin, which is found in the exoskeletons of arthropods. Chitosan is structurally similar to glycosaminoglycans and is enzymatically degradable. Ionic or chemical cross-linking methods can be used to form chitosan hydrogels (Lee and Mooney, 2001; Drury and Mooney, 2003; Peppas et al, 2006).

Poly(HEMA) hydrogels have been used in contact lenses and drug delivery devices. PNIPAAm is a temperature-responsive polymer. The lower critical solution temperature (LCST) of PNIPAAm in water is 32°C, and PNIPAAm solutions transition to form hydrogels at temperatures above the LCST. PNIPAAm hydrogels have been used to culture cell sheets because the thermal-responsive nature of PNIPAAm allows the cell sheets to be easily isolated by decreasing the temperature of the cell-hydrogel construct (Lee and Mooney, 2001; Drury and Mooney, 2003; Peppas et al, 2006).

1.1.1.1 Alginate

Alginate is linear polysaccharide derived from brown algae. Alginate chains consist of blocks of (1,4)-linked β -D-mannuronic acid (M) and α -L-guluronic acid (G). Both the molecular weight and the ratio of M and G blocks can be varied to control the properties of alginate

hydrogels. Carbodiimide chemistry can be used to functionalize alginate molecules by linking molecules with amine groups to carboxylate groups on the alginate backbone. Alginate has been widely used in the food industry as an emulsifier and gelling agent. As a biomaterial, alginate has been used in drug delivery, cell encapsulation, dental impressions, and wound dressings. For tissue engineering applications, alginate is frequently functionalized to present cell adhesion peptides since alginate hydrogels are inherently inert to cell adhesion (Augst et al, 2006). The feasibility of using alginate as a synthetic ECM was first demonstrated in 1999 when Arginine-Glycine-Aspartic Acid (RGD) cell adhesion peptides were conjugated to alginate hydrogels (Rowley et al, 1999).

To form alginate hydrogels, multivalent cations, such as Ca^{2+} can be used to cross-link the G blocks in alginate molecules. With this approach, the mechanical stiffness of the resulting alginate hydrogel can be controlled with the cation concentration (Augst et al, 2006). Furthermore, ionically cross-linked alginate hydrogels can be readily dissolved using a chelating agent such as ethylenediaminetetraacetic acid (EDTA) (Doner and Becard, 1991). Alternatively, alginate hydrogels can be formed with covalent cross-linking using carbodiimide chemistry. Recently, photopolymerizable alginate hydrogels have been synthesized. In this approach, carbodiimide chemistry is first used to conjugate acrylate groups to alginate molecules. The modified alginate molecules are then mixed with photoinitiator and cross-linked with ultraviolet light (Jeon et al, 2009; Cha et al, 2009).

The mechanical properties of alginate hydrogels can be controlled with the type and concentration of cross-linker, the concentration of alginate molecules, and the molecular weight of alginate molecules. Increasing the concentration of alginate molecules yields stiffer gels but also increases the viscosity of the pre-gelled solution which may be undesirable, especially for

cell encapsulation in which an increase in solution viscosity will lead to increased shear stresses on the cells and decreased cell viability (Augst et al, 2006). To increase the stiffness of alginate hydrogels without significantly increasing the viscosity of the pre-gel solution, low molecular weight alginate can be used. Low molecular weight alginate allows the viability of cells to be maintained during encapsulation despite increases in alginate concentration and subsequent hydrogel stiffness (Kong et al, 2003). Furthermore, by varying the ratio between high molecular weight and low molecular weight alginate, the viscosity of the pre-gel solution can be decoupled from the stiffness of the resulting alginate hydrogels (Kong et al, 2002). Incorporation of alginate modified with methacrylic groups has also been shown to control the mechanical properties of other hydrogel systems, including poly(ethylene glycol) diacrylate (PEGDA) and polyacrylamide (Jeong et al, 2011).

The degradation properties of alginate hydrogels can be controlled with the molecular weight of alginate molecules or chemical modifications to the alginate backbone. Ionically cross-linked alginate hydrogels will dissolve in neutral pH as the divalent cross-linkers diffuse (Augst et al, 2006). For more controlled degradation, the molecular weight distribution of the pre-gel solution can be controlled. Incorporation of low molecular weight alginate increases the degradation kinetics of alginate hydrogels (Kong et al, 2004). In addition, the alginate backbone can be oxidized with sodium periodate to expose hydrolytically labile bonds (Boontheekul et al, 2005). Further modification of the oxidized alginate with methacrylic groups can be used to control degradation behavior of other hydrogel systems, including PEGDA, and facilitate the reorganization of encapsulated cells (Zorlutuna et al, 2011).

1.1.1.2 Poly(ethylene glycol)

Poly(ethylene glycol) (PEG) is a variation of poly(ethylene oxide) (PEO), which is one of the most common synthetic polymers used in tissue engineering. Due to its biocompatibility and low toxicity, PEO has been approved by the Food and Drug Administration (FDA) for several medical applications. PEO is an extremely hydrophilic polymer and can be chemically modified to contain enzymatically-cleavable or hydrolytically-degradable sequences. It has also been modified to contain acrylate groups so hydrogels can be formed through photopolymerization.

PEG is a biocompatible, inert, hydrophilic polymer. PEG hydrogels are frequently formed from photopolymerizations of acrylate-terminated PEG monomers (Peppas et al, 2006). Photopolymerizable PEG has been used in various applications including cell encapsulation and drug delivery (Ifkovits and Burdick, 2007). In order to promote cell spreading on and within PEG hydrogels, researchers have modified RGD cell adhesion peptides with acrylate moieties for incorporation into PEG diacrylate hydrogels (Hern and Hubbell, 1997; Burdick and Anseth, 2002). Degradable linkages can be incorporated in the PEG backbone to yield degradable PEG hydrogels. For example, α -hydroxy acid oligomers have been incorporated in between the PEG and photoreactive groups to yield hydrolytically degradable PEG chains (Sawhney et al, 1993). Using a similar strategy, proteolytically degradable groups have also been incorporated in the PEG backbone to facilitate degradation (West and Hubbell, 1999).

1.1.2 Stem cells in tissue engineering

One of the significant challenges in the field of tissue engineering has been finding viable cell sources. Stem cells have the ability to differentiate into specific cell types or lineages, and this pluripotent nature of stem cells makes them attractive for tissue regeneration applications

(Khademhosseini et al, 2006; Badylak and Nerem, 2010). Adult stem cells can be isolated from various tissues in the body, including bone marrow and fat tissue. Embryonic stem cells (ESCs), isolated from the inner cell mass of a developing blastocyst, are capable of differentiating into any cell type, but the use of ESCs has been hindered by poor controllability of self-renewal and differentiation as well as ethical concerns. For stem cells to be used effectively in tissue engineering, the necessary number of cells with the appropriate phenotype must be obtained (Mikos et al, 2006; Polak and Bishop, 2006). Towards this end, stem cell niches are being extensively studied in efforts to develop synthetic stem cell niches to control the proliferation and differentiation of stem cells (Lutolf and Blau, 2009).

Separately, much research is focused on identifying, purifying, and expanding adult stem cell populations for tissue engineering applications (Lutolf and Blau, 2009). Hematopoietic stem cells (HSCs) are multipotent cells that can give rise to all the cell types found in blood. HSCs have also been shown to differentiate into liver cells (Lagasse 2000). Stem cells isolated from blood have been shown to undergo osteogenic differentiation (Kuznetsov et al, 2001). Endothelial progenitor cells (EPCs), which are isolated from peripheral blood or cord blood, have been investigated for vascular tissue engineering applications (Riha et al, 2005).

Mesenchymal stem cells (MSCs) are another population of adult stem cells that have been widely used in tissue engineering due to their potential to differentiate into mesenchymal tissues, including bone, ligament, cartilage, and muscle. For vascular engineering, MSCs can be differentiated into smooth muscle and endothelial cell types to engineer new blood vessels (Riha et al, 2005). For bone tissue engineering, researchers have combined MSCs with biomaterial scaffolds that can be implanted in bone defects to promote tissue regeneration and defect repair. This approach has been shown to improve bone formation *in vivo*, and it has been proposed that

the therapeutic effects of implanted MSCs are related both to an increased number of progenitor cells and also osteogenic factors secreted by the cells. MSCs can also be cultured within biomaterial scaffolds *in vitro* to promote osteogenic differentiation and bone formation prior to implantation *in vivo*. In addition, MSCs have been transplanted without the use of biomaterial scaffolds to treat musculoskeletal diseases such as osteoporosis. Despite promising results, the use of MSCs has been limited by difficulties in expanding MSCs to clinically useful numbers while maintaining their differentiation potential (Mauney et al, 2005).

1.2 Synthetic extracellular matrices

The extracellular matrix (ECM) is a major component of cellular microenvironments, which also consist of surrounding cells and soluble factors. Crosstalk between the extracellular matrix and the cell cytoskeleton has been shown to regulate cell behavior including migration, morphogenesis, proliferation, differentiation, and death (Lutolf and Hubbell, 2005). Cells attach to the surrounding matrix through integrins which interact with the actin cytoskeleton in the cell interior. Focal adhesions are the most well-characterized cell-matrix adhesions and are located near the periphery of cells (Geiger et al, 2001). For stem cells, the cellular microenvironment is also known as a stem cell niche, and the surrounding ECM is involved in stem cell proliferation and differentiation (Lutolf and Blau, 2009).

Synthetic ECMs have been synthesized to direct cellular behavior and function and also to study cell-matrix interactions *in vitro* in efforts to gain a better understanding of the interactions between cells and their microenvironments. Naturally-derived hydrogel polymers are well-suited for use as synthetic ECMs due to their similarity to the native ECM. While useful in clinical applications, naturally-derived polymers exhibit poor controllability and are

thus not well-suited for scientific studies to investigate cell-matrix interactions. Synthetic materials can be modified to mimic the natural ECM and frequently allow for more controllability than naturally-derived polymers. In order to serve as ECMs, synthetic materials must be modified with the appropriate biological cues, including cell adhesion domains for integrin binding. Additional bioactive domains may also be needed, including binding sites for growth factors and enzymatically-degradable sequences (Lutolf and Hubbell, 2005).

Synthetic ECMs can be designed to support cells in two-dimensional (2D) or three-dimensional (3D) cultures. To more accurately mimic the natural ECM, much research is currently focused on developing 3D synthetic ECMs (Lutolf and Hubbell, 2005; Griffith and Swartz, 2006). Synthetic ECMs have also been considered for use in testing molecular therapeutics. *In vitro* testing of molecular therapeutics has often been a poor predictor of *in vivo* responses, possibly due to differences in the cellular microenvironment between *in vitro* and *in vivo* conditions (Bhadriraju and Chen, 2002). Changes in the cellular microenvironment have been shown to alter the cellular response to molecular therapeutics, and the properties and structure of the ECM are known to change with disease and trauma (Kong and Mooney, 2007). Synthetic ECMs with tunable properties would thus be useful for *in vitro* testing of molecular therapeutics. Overall, much research has been focused on the design and development of synthetic ECMs with particular emphasis on the effects of stiffness and cell adhesion ligands presented by synthetic ECMs.

1.2.1 Effects of matrix stiffness on cell behavior

The stiffness of a material can be measured with its elastic modulus, which quantifies the tendency of a material to deform upon application of an external stress. More specifically, the

elastic modulus is defined as the slope of the stress-strain curve of a material upon elastic deformation. Tissues in the body span a wide range of elastic moduli; for example, brain tissue has an elastic modulus around 1 kPa while collagenous bone has an elastic modulus around 100 kPa. Cells are able to sense and respond to ECM stiffness by pulling on and deforming the matrix. Matrix stiffness has been shown to influence a wide range of cell behavior, including contractility, motility, and spreading (Discher et al, 2005).

The effects of matrix stiffness on cell behavior were first demonstrated using epithelial cells and fibroblasts cultured on collagen-coated polyacrylamide hydrogels (Pelham and Wang, 1997). Since then, much research has been focused on the effects of matrix stiffness on various cell behavior and function. The proliferation and differentiation of preosteoblasts were regulated by substrate stiffness, as cells exhibited increased proliferation and decreased differentiation when cultured on gels of increasing stiffness (Kong et al, 2005). Substrate stiffness was also shown to influence preosteoblast migration, focal adhesion formation, and cytoskeletal organization (Khatriwala et al, 2006). Mesenchymal stem cells have been shown to differentiate to various lineages based on the stiffness of the substrate on which they are cultured (Engler et al, 2006). Substrate stiffness has also been shown to influence cell spreading, actin cytoskeleton formation and integrin expression (Yeung et al, 2005).

1.2.2 Effects of cell adhesion cues on cell behavior

Interactions between cells and their surrounding ECM are governed by cell-matrix binding through integrins on the cell surface. These cell-matrix binding interactions influence intracellular signaling and gene expression, thus controlling cell function. Synthetic ECMs with varied density, spacing, and conformation of cell adhesion ligands have been used in efforts to

better understand these cell-matrix binding interactions that are known to influence various cell processes (Kong et al, 2006).

The density of cell adhesion peptides incorporated in synthetic ECMs was shown to influence the proliferation and differentiation of myoblasts cultured on a 2D synthetic ECM (Rowley and Mooney, 2002) as well as the proliferation and differentiation of pre-osteoblasts and myoblasts cultured within a 3D synthetic ECM (Kong et al, 2006). The proliferation and differentiation of pre-osteoblasts cultured on hydrogel substrates were increased by decreasing the spacing of cell adhesion ligands in the synthetic ECM (Lee et al, 2004). Furthermore, the spacing of cell adhesion ligands incorporated in synthetic ECMs influenced integrin-ligand bond formation for cells cultured on 2D while having little effect on integrin-ligand bond formation for cells cultured in a 3D synthetic ECM (Hsiong et al, 2008). The conformation of cell adhesion peptides in synthetic ECMs has also been shown to influence cell behavior (Hsiong et al, 2009).

1.3 Gene therapy

Gene therapy refers to the transfer of genetic material in efforts to treat disease (Glover et al, 2005; Pack et al, 2005). Gene therapy can be used to replace defective genes in the treatment of genetic diseases, such as cystic fibrosis, haemophilia, or muscular dystrophy, or be used to deliver therapeutic proteins in the treatment of acquired diseases, such as cancer or cardiovascular disease (Pack et al 2005; Edelstein et al, 2007). In tissue engineering applications, therapeutic genes can be delivered in efforts to repair lost or damaged tissues (Storrie and Mooney, 2006; De Laporte and Shea, 2007; O'Rourke et al, 2010). The success of

gene therapy depends on safely delivering the appropriate genes to target cells to induce the necessary expression profiles and ultimately achieve therapeutic efficacy (Pack et al, 2005).

1.3.1 Delivery of therapeutic genes

Gene delivery vectors are used to package therapeutic genes for delivery to host cells and can generally be classified as viral or non-viral vectors (Pack et al, 2005). Due to safety concerns associated with viral vectors, including immunogenicity and mutagenesis resulting from insertions of the viral genome into the genome of the host cell (Glover et al, 2005), much research has focused on the use of non-viral vectors for gene delivery. The majority of non-viral vectors have been synthesized from lipids, polymers, or polypeptides. These materials typically contain cationic groups that electrostatically bind to and condense genes to form polyplexes, which protect the genes and facilitate their entry to target cells. Poly(ethyleneimine) (PEI) is a widely used polymer for non-viral gene delivery. Unfortunately, the use of non-viral vectors has thus far been limited by low gene-transfer efficiencies *in vivo* (Pack et al, 2005).

Therapeutic genes can be delivered to the body through a variety of administration routes including intramuscular injection, intravenous injection, and subcutaneous administration (Pouton et al, 2001; Herweijer and Wolff, 2003). Delivered genes must first overcome a variety of extracellular and intracellular barriers before expression by target cells can be achieved. In the bloodstream, the majority of delivered genes are quickly cleared through the liver or degraded by plasma nucleases before reaching the target cells. Targeting the appropriate host cells may be another hurdle, and much research has focused on conjugating targeting cues to gene delivery vectors for increased cell-specificity. Once the polyplex has reached the cells, the complex must be internalized, typically through endocytosis. The polyplex must then escape the

endosome, transport through the cytoplasm, and enter the nucleus to begin transcription. In order for the gene to be expressed, it must also be unpackaged from the delivery vehicle after entry into the cell. These barriers are not insignificant, as evidenced by low expression efficiency despite high gene uptake. Low gene transfer efficiency *in vivo* is one of the major hurdles to effective non-viral gene delivery for therapeutic applications (Pack et al, 2005; Wiethoff and Middaugh, 2003). In efforts to improve gene transfer efficiency, much research has been focused on designing and synthesizing gene delivery vectors (Leong et al, 1998; Fischer et al, 1999; Forrest et al, 2003; Mintzer and Simanek 2003).

1.3.2 Gene therapy in tissue engineering

Tissue engineering strategies typically require the use of cytokines or growth factors to stimulate tissue regeneration. Direct protein delivery, however, is problematic due to issues such as limited protein stability. Gene delivery is an attractive alternative to protein delivery for tissue engineering applications, as genes can be used to stimulate therapeutic protein production. For tissue engineering, both viral and non-viral vectors have been used with varying success. As with all gene therapies, one of the challenges to using therapeutic genes in tissue engineering is activating target cells to express the needed amount of therapeutic protein for the appropriate duration (Heyde et al, 2007). For tissue regeneration, growth factor signaling is typically desired only at the defect site and typically required for only a few weeks (Storrie and Mooney, 2006).

For tissue engineering applications, therapeutic genes can be delivered *in vivo* or *ex vivo*. *In vivo* delivery refers to the delivery of therapeutic genes directly to the body, typically at the site of interest. The genes can either be directly injected to the target site or encapsulated in a scaffold for implantation at the target site. In the latter strategy, the scaffold can serve as a

delivery depot while protecting the encapsulated genes from degradation. For *ex vivo* delivery, cells, which can be isolated from the patient, are transfected with the therapeutic gene *in vitro* and then transplanted at the site of interest. Transfected cells can be delivered by direct injection or incorporated in biomaterial scaffolds for transplantation (Heyde et al, 2007).

Much research has focused on the use of biomaterial scaffolds as gene delivery depots for tissue engineering applications (Storrie and Mooney, 2006). Genes can be incorporated into polymer scaffolds with or without delivery vectors; for example, plasmid DNA can either be incorporated directly into a scaffold or condensed with a cationic polymer prior to incorporation. Gene delivery vectors can be physically immobilized in the hydrogel scaffold through non-specific binding, such as van der Waals, hydrophobic, or electrostatic interactions, or through chemical coupling. Vectors that interact with the scaffold through non-specific binding can be released through desorption while vectors that are chemically linked to the scaffold are released upon degradation of the linkage (De Laporte and Shea 2007).

Another critical issue in gene delivery is the effect of the cellular microenvironment (Kong and Mooney, 2007). Recent studies have shown that matrix stiffness plays a role in regulating non-viral gene delivery. Pre-osteoblasts cultured on hydrogel-based cell adhesion substrates demonstrated an increase in the uptake and expression of plasmid DNA as the stiffness of the substrates was increased (Kong et al, 2005). In addition to substrate stiffness, the density and spacing of cell adhesion ligands has been shown to influence non-viral gene delivery. Gene transfer to and subsequent expression from pre-osteoblasts cultured on hydrogel-based cell adhesion substrates increased as the density of cell adhesion ligands was increased and the spacing of cell adhesion ligands was decreased (Kong et al, 2006).

1.4 Project overview

The work described in this thesis focuses on the development of synthetic ECMs for stem cell culture and gene delivery. Overall, the objective of this work was to evaluate design parameters for synthetic ECMs to facilitate the use of stem cells and therapeutic genes for tissue engineering applications. First, in Chapter 2, the development of a synthetic stem cell niche for spermatogonial stem cell culture (SSC) will be described. The subsequent two chapters, Chapters 3 and 4, focus on designing synthetic ECMs for gene delivery. The effects of matrix stiffness on non-viral gene delivery to fibroblasts, bone marrow stromal cells (BMSCs), and myoblasts will be outlined followed by the development of a synthetic ECM with angiogenic gene therapy for revascularization. Ultimately, the results from these studies will be useful for developing advanced tissue engineering strategies for clinical settings.

1.5 References

1. Augst AD, Kong HJ, Mooney DJ. Alginate hydrogels as biomaterials. *Macromolecular Bioscience* 6, 623, 2006.
2. Badylak SF and Nerem RM. Progress in tissue engineering and regenerative medicine. *Proceedings of the National Academy of Sciences USA* 107, 3285, 2010.
3. Boonthekul T, Kong HJ, Mooney DJ. Controlling alginate gel degradation utilizing partial oxidation and bimodal molecular weight distribution. *Biomaterials* 26, 2455, 2005.
4. Burdick JA, Anseth KS. Photoencapsulation of osteoblasts in injectable RGD-modified PEG hydrogels for bone tissue engineering. *Biomaterials* 23, 4315, 2002.
5. Cha C, Kohman RE, Kong H. Independent control of stiffness, toughness, and hydrogel degradation rate. *Advanced Functional Materials* 19, 3056, 2009.
6. De Laporte L and Shea LD. Matrices and scaffolds for DNA delivery in tissue engineering. *Advanced Drug Delivery Reviews* 59, 292, 2007.
7. Discher DE, Janmey P, and Wang YL. Tissue cells feel and respond to the stiffness of their substrate. *Science* 310, 1139, 2005.
8. Doner LW and Becard G. Solubilization of gellan gels by chelation of cations. *Biotechnology Techniques* 5, 25, 1991.
9. Drury JL and Mooney DJ. Hydrogels for tissue engineering: scaffold design variables and applications. *Biomaterials* 24, 4337, 2003.
10. Edelstein ML, Abedi MR, and Wixon J. Gene therapy clinical trials worldwide to 2007 – an update. *The Journal of Gene Medicine* 9, 833, 2007.
11. Engler AJ, Sen S, Sweeney HL, Discher DE. Matrix elasticity directs stem cell lineage specification. *Cell* 126, 677, 2006.
12. Fischer D, Bieber T, Li Y, Elsässer HP, and Kissel T. A novel non-viral vector for DNA delivery based on low molecular weight, branched polyethylenimine: Effect of molecular weight on transfection efficiency and cytotoxicity. *Pharmaceutical Research* 16, 1273, 1999.
13. Forrest ML, Koerber JT, and Pack DW. A degradable polyethylenimine derivative with low toxicity for highly efficient gene delivery. *Bioconjugate Chemistry* 14, 934, 2003.
14. Geiger B, Bershadsky A, Pankov R, Yamada KM. Transmembrane extracellular matrix-cytoskeleton crosstalk. *Nature Reviews Molecular Cell Biology* 2, 793, 2001.

15. Glover DJ, Lipps HJ, and Jans DA. Towards safe, non-viral therapeutic gene expression in humans. *Nature Reviews Genetics* 6, 299, 2005.
16. Griffith LG and Naughton G. Tissue engineering – current challenges and expanding opportunities. *Science* 295, 1009, 2002.
17. Griffith LG and Swartz MA. Capturing complex 3D tissue physiology in vitro. *Nature Reviews Molecular Cell Biology* 7, 211, 2006.
18. Hern DL and Hubbell JA. Incorporation of adhesion peptides into nonadhesive hydrogels useful for tissue resurfacing. *Journal of Biomedical Materials Research* 39, 266, 1998.
19. Herweijer H and Wolff JA. Progress and prospects: naked DNA gene transfer and therapy. *Gene Therapy* 10, 453, 2003.
20. Heyde M, Partridge KA, Oreffo ROC, Howdle SM, Shakesheff KM, Garnett MC. Gene therapy used for tissue engineering applications. *Journal of Pharmacy and Pharmacology* 59, 329, 2007.
21. Hirano Y and Mooney DJ. Peptide and protein presenting materials for tissue engineering. *Advanced Materials* 16, 17, 2004.
22. Hsiong SX, Boontheekul T, Huebsch N, Mooney DJ. Cyclic arginine-glycine-aspartate peptides enhance three-dimensional stem cell osteogenic differentiation. *Tissue Engineering Part A* 15, 263, 2009.
23. Hsiong SX, Huebsch N, Fischbach C, Kong HJ, Mooney DJ. Integrin-adhesion ligand bond formation of preosteoblasts and stem cells in three-dimensional RGD presenting matrices. *Biomacromolecules* 9, 1843, 2008.
24. Ifkovits JL and Burdick JA. Review: photopolymerizable and degradable biomaterials for tissue engineering applications. *Tissue Engineering* 13, 2369, 2007.
25. Jeon O, Bouhadir KH, Mansour JM, Alsberg E. Photocrosslinked alginate hydrogels with tunable biodegradation rates and mechanical properties. *Biomaterials* 30, 2724, 2009.
26. Jeong JH, Chan V, Cha C, Zorlutuna P, Dyck C, Hsia KJ, Bashir R, Kong H. “Living” microvascular stamp for patterning of functional neovessels; orchestrated control of matrix property and geometry. *Advanced Materials*, 2011.
27. Khademhosseini A, Vacanti JP, Langer R. Progress in tissue engineering. *Scientific American* 300, 64, 2009.
28. Khademhosseini A, Langer R, Borenstein J, Vacanti JP. Microscale technologies for tissue engineering and biology. *Proceedings of the National Academy of Sciences USA* 103, 2480, 2006.

29. Khatiwala CB, Peyton SR, Putnam AJ. Intrinsic mechanical properties of the extracellular matrix affect the behavior of pre-osteoblastic MC3T3-E1 cells. *American Journal of Physiology – Cell Physiology* 290, C1640, 2006.
30. Kong HJ and Mooney DJ. Microenvironmental regulation of biomacromolecular therapies. *Nature Reviews Drug Discovery* 6, 455, 2007.
31. Kong HJ, Boontheekul T, Mooney DJ. Quantifying the relation between adhesion ligand-receptor bond formation and cell phenotype. *Proceedings of the National Academy of Sciences USA* 103, 18534, 2006.
32. Kong HJ, Kaigler D, Kim K, Mooney, DJ. Controlling rigidity and degradation of alginate hydrogels via molecular weight distribution. *Biomacromolecules* 5, 1720, 2004.
33. Kong HJ, Lee KY, Mooney DJ. Decoupling the dependence of rheological/mechanical properties of hydrogels from solids concentration. *Polymer* 43, 6239, 2002.
34. Kong HJ, Liu JD, Riddle K, Matsumoto T, Leach K, Mooney DJ. Non-viral gene delivery regulated by stiffness of cell adhesion substrates. *Nature Materials* 4, 460, 2005.
35. Kong HJ, Polte TR, Alsberg E, Mooney DJ. FRET measurements of cell-traction forces and nano-scale clustering of adhesion ligands varied by substrate stiffness. *Proceedings of the National Academy of Sciences USA* 102, 4300, 2005.
36. Kong HJ, Smith MK, Mooney DJ. Designing alginate hydrogels to maintain viability of immobilized cells. *Biomaterials* 24, 4023, 2003.
37. Kuznetsov SA, Mankani MH, Gronthos S, Satomura K, Bianco P, Robey PG. Circulating skeletal stem cells. *The Journal of Cell Biology* 153, 1133, 2001.
38. Lagasse E, Connors H, Al-Dhalimy M, Reitsma M, Dohse M, Osborne L, Wang X, Finegold M, Weissman IL, Grompe M. Purified hematopoietic stem cells can differentiate into hepatocytes in vivo. *Nature Medicine* 6, 1229, 2000.
39. Langer R and Vacanti JP. Tissue engineering. *Science* 260, 920, 1993.
40. Lee KY and Mooney DJ. Hydrogels for tissue engineering. *Chemical Reviews* 101, 1869, 2001.
41. Lee KY, Alsberg E, Hsiong S, Comisar W, Linderman J, Ziff R, Mooney D. Nanoscale adhesion ligand organization regulates osteoblast proliferation and differentiation. *Nano Letters* 4, 1501, 2004.
42. Leong KW, Mao HQ, Truong-Le VL, Roy K, Walsh SM, and August JT. DNA-polycation nanospheres as non-viral gene delivery vehicles. *Journal of Controlled Release* 53, 183, 1998.

43. Lutolf MP, Hubbell JA. Synthetic biomaterials as instructive extracellular microenvironments for morphogenesis in tissue engineering. *Nature Biotechnology* 23, 47, 2005.
44. Mauney JR, Volloch V, Kaplan DL. Role of adult mesenchymal stem cells in bone tissue-engineering applications: current status and future prospects. *Tissue Engineering* 11, 787, 2005.
45. Mintzer MA and Simanek EE. Nonviral vectors for gene delivery. *Chemical Reviews* 109, 259, 2009.
46. O'Rourke S, Keeney M, and Pandit A. Non-viral polyplexes: scaffold mediated delivery for gene therapy. *Progress in Polymer Science* 35, 441, 2010.
47. Pack DW, Hoffman AS, Pun S, and Stayton PS. Design and development of polymers for gene delivery. *Nature Reviews Drug Discovery* 4, 581, 2005.
48. Pelham RJ and Wang YL. Cell locomotion and focal adhesions are regulated by substrate flexibility. *Proceedings of the National Academy of Sciences USA* 94, 13661, 1997.
49. Zorlutuna P, Jeong JH, Kong H, Bashir R. Stereolithography-Based Hydrogel Microenvironments to Examine Cellular Interactions. *Advanced Functional Materials* 21, 3642, 2011.
50. Pouton CW and Seymour LW. Key issues in non-viral gene delivery. *Advanced Drug Delivery Reviews* 46, 187, 2001.
51. Ratner BD and Bryant SJ. Biomaterials: where we have been and where we are going. *Annual Review of Biomedical Engineering* 6, 41, 2004.
52. Riha GM, Lin PH, Lumsden AB, Yao QZ, Chen CY. Application of stem cells for vascular tissue engineering. *Tissue Engineering* 11, 2535, 2005.
53. Rowley JA and Mooney DJ. Alginate type and RGD density control myoblast phenotype. *Journal of Biomedical Materials Research* 60, 217, 2002.
54. Rowley JA, Madlambayan G, Mooney DJ. Alginate hydrogels as synthetic extracellular matrix materials. *Biomaterials* 20, 45, 1999.
55. Sawhney AS, Pathak CP, Hubbell JA. Bioerodible hydrogels based on photopolymerized poly(ethylene glycol)-co-poly(alpha-hydroxy acid) diacrylate macromers. *Macromolecules* 26, 581, 1993.
56. Schmidt JJ, Rowley J, Kong HJ. Hydrogels used for cell-based drug delivery. *Journal of Biomedical Materials Research A* 87A, 1113, 2008.

57. Storrie H and Mooney DJ. Sustained delivery of plasmid DNA from polymeric scaffolds for tissue engineering. *Advanced Drug Delivery Reviews* 58, 500, 2006.
58. West JL and Hubbell JA. Polymeric biomaterials with degradation sites for proteases involved in cell migration. *Macromolecules* 32, 241, 1999.
59. Wiethoff CM and Middaugh CR. Barriers to nonviral gene delivery. *Journal of Pharmaceutical Sciences* 92, 203, 2003.
60. Yeung T, Georges PC, Flanagan LA, Marg B, Ortiz M, Funaki M, Zahir N, Ming WY, Weaver V, Janmey PA. Effects of substrate stiffness on cell morphology, cytoskeletal structure, and adhesion. *Cell Motility and the Cytoskeleton* 60, 24, 2005.

CHAPTER 2: THREE-DIMENSIONAL SYNTHETIC NICHE FOR SPERMATOGONIAL STEM CELL CULTURE*

2.1 Introduction

The use of stem cells in efforts to repair tissues and organs has become increasingly prevalent in the field of tissue engineering. Stem cells reside in specialized microenvironments, or niches, which regulate their self-renewal and overall maintenance (Schofield, 1978; Watt and Hogan, 2000). In order to best utilize the therapeutic potential of stem cells, it is crucial to understand the interactions between stem cells and their native environment to define optimal niches for therapeutic applications (Gumbiner, 1996; Griffith and Swartz, 2006). Significant progress has been made in characterizing the niche microenvironment of a variety of stem cells; more specifically, recent studies have investigated the hematopoietic, epidermal, intestinal, and neural stem cell niches (Li and Xie, 2005; Moore and Lemischka, 2006). Within each niche, supporting cells and associated blood vessels produce the necessary growth factors and stimuli that will modulate stem cell behavior. In addition, the extracellular matrix (ECM) is responsible for cell attachment and can also regulate cellular response to surrounding stimuli (Discher et al, 2005; Geiger et al, 2001). Therefore, the composition of the ECM and the interactions between cells and their surrounding matrix are crucial in regulating stem cell fate.

Stem cells belonging to epithelial structures generally reside on a specialized ECM called the basement membrane. Although composed of a small set of specific proteins such as collagen IV, laminin, entactin, fibronectin and perlecan, the basement membrane shows an impressive

* This chapter contains work previously published in *Tissue Engineering* and is reprinted here with the permission of Mary Ann Liebert, Inc. This work was previously published as Chu C, Schmidt JJ, Carnes K, Zhang Z, Kong HJ, Hofmann MC. Three-dimensional synthetic niche components to control germ cell proliferation. *Tissue Engineering* 15, 255, 2009.

tissue- and site-specific variability in its composition (McMillan et al, 2003). Maintenance of stemness, proliferation, and migration take place in the basal layer of epithelia, in contact with the basement membrane. These biological activities are regulated in part through interactions between individual components of the basement membrane and cell surface receptors called integrins (Giancotti and Ruoslahti, 1999; Erickson and Couchman, 2000). Integrins recognize and bind various ECM proteins, including those that contain the Arg-Gly-Asp (RGD) peptide sequence (Pierschbacher and Ruoslahti, 1984; Gardner and Hynes, 1985).

Biomaterials have been increasingly used to simulate and even modulate cell adhesion to the ECM in order to regulate signaling pathways controlling cell function and tissue morphogenesis. For this purpose, biomaterials have been designed to mimic the biochemical and biomechanical properties of the natural ECM (Lee and Mooney, 2001; Luotlf and Hubbell, 2005; Stevens and George, 2005). Extensive chemical modifications have been used to incorporate synthetic cell adhesion oligopeptides into biomaterials, and the spatial organization of these cell adhesion cues at the nanometer and micrometer scale has been used to modulate the function of progenitor and precursor cells (Rowley and Mooney, 2002; Lee et al, 2004; Kong et al, 2005; Kong et al, 2007). In addition, the mechanical stiffness of biomaterials to which cells are adhered has been shown to significantly regulate the phenotypes of precursor cells (Kong et al, 2006; Boontheekul et al, 2007).

Mammalian spermatogenesis is a tightly regulated and continuous process in which spermatogonial stem cells (SSCs) self-renew and differentiate to ultimately form spermatozoa. The SSC niche is found within the seminiferous epithelium where nursing Sertoli cells provide structural support and growth factors to the stem cells. Other stimuli are provided by the vascular network and interstitial cells between the seminiferous tubules (Yoshida et al, 2007).

Another important component of the testicular niche is the basement membrane, to which stem cells and Sertoli cells are attached through integrins. In 2004, the group of T. Shinohara demonstrated that mouse SSCs can dedifferentiate *in vitro*, reverting into cells that acquire an ES cell phenotype (Kanatsu-Shinohara et al, 2004). These ES-like cells can then be differentiated into cells belonging to the three embryonic germ layers. More recently, the same potential for pluripotency has been demonstrated for adult SSCs (Guan et al, 2006). Therefore, SSCs could potentially be used to regenerate and engineer specific tissues in an autologous manner. While progress has been made recently in expanding SSCs *in vitro* using cocktails of growth factors (Kubota et al, 2004; Kanatsu-Shinohara et al, 2005), growing and maintaining these cells *in vitro* can be further optimized. Therefore, other niche parameters that are important for SSC proliferation *in vitro*, specifically the composition of the extracellular matrix, need to be characterized.

2.2 Objective and scope

In the present study, we hypothesize that a bioactive hydrogel designed to mimic some of the biochemical and biomechanical properties of the basement membrane can be used as part of a synthetic niche; by mimicking the *in vivo* niche, such a synthetic niche can be used to regulate SSC proliferation. This study presents an initial set of parameters that has been known to significantly regulate the phenotypes of precursor cells, namely cell adhesion ligand density and mechanical properties. Calcium cross-linked alginate hydrogels, which do not naturally facilitate protein absorption and cell adhesion (Smetana, 1993; Rowley et al, 1999) were chemically coupled with synthetic oligopeptides containing the Arg-Gly-Asp (RGD) sequence (RGD peptides) in order to control the number of cell adhesion sites for a spermatogonial stem cell line.

As a model for SSCs, the C18-4 spermatogonial cell line was used (Hofmann et al, 2005). This cell line exhibits many of the characteristics of normal spermatogonial stem cells, including the expression of the GFR α -1/Ret membrane receptor complex that binds the growth factor glial cell line-derived neurotrophic factor (GDNF). Upon stimulation with GDNF, the cells increase their rate of proliferation, which is mediated by Src and Ras-dependent signaling pathways (Braydich-Stolle et al, 2007; He et al, 2008). The mechanical stiffness of the hydrogels was varied from 8 – 110 kPa, which is within the stiffness range of the natural basement membrane (Lu et al, 2004; Candiello et al, 2007), to examine the effects of matrix stiffness on SSC behavior. The hydrogel properties were first optimized through cell culture on two-dimensional (2D) hydrogel surfaces; cell adhesion and proliferation were then subsequently examined in three-dimensional (3D) hydrogel systems.

2.3 Materials and methods

2.3.1 Alginate modification

Sodium alginate (FMC Biopolymer, Philadelphia, PA) was used as high molecular weight alginate ($M_w \sim 250,000$ g/mol). Low molecular weight alginate ($M_w \sim 60,000$ g/mol) was obtained by irradiating the sodium alginate with a cobalt-60 source for 4 hours at a dose of 5.0 Mrad (Kong et al, 2002). Alginate molecules were covalently coupled with (Gly)₄-Arg-Gly-Asp-Ala-Ser-Ser-Lys (G₄RGDASSKY) oligopeptides (Peptides International, Louisville, KY) using a carbodiimide chemistry as previously described (Figure 2.1; Rowley et al, 1999). The mole ratio between RGD peptides and alginate was kept constant at 2:1. All alginate solutions were filtered, lyophilized, and reconstituted with Dulbecco's Modified Eagle's Medium (DMEM, Invitrogen Corporation, Carlsbad, CA) to obtain a 2% w/v solution prior to gelation.

2.3.2 Cell line and cell culture

The C18-4 cell line was established by stably transfecting undifferentiated type A spermatogonia with the Large T antigen gene driven by the ecdysone promoter (Hofmann et al, 2005). These cells exhibit many features of spermatogonial stem cells, including the expression of Oct-4, Vasa, and the receptor complex for glial cell line-derived neurotrophic factor (GDNF), a crucial stimulus for self-renewal (Braydich-Stolle et al, 2007; He et al, 2008). Cells were cultured in DMEM supplemented with 10% fetal bovine serum (FBS, Invitrogen Corporation, Carlsbad, CA) and 100 units/ml penicillin-streptomycin (Invitrogen Corporation, Carlsbad, CA) at 37° C in a 5% CO₂ incubator. The cell culture medium was changed every other day.

2.3.3 Two-dimensional cell culture on hydrogels

High molecular weight alginate was used for two-dimensional (2D) cell culture studies. Gels with 3 different densities of cell adhesion peptides were made by mixing unmodified high molecular weight alginate with G₄RGDASSKY-conjugated high molecular weight alginate in ratios of 9:1, 1:1, and 1:9. Alginate hydrogels were formed with ionic cross-linking (Figure 2.2) by mixing alginate solutions with a 20% (w/w) calcium sulfate (CaSO₄, Sigma Aldrich, St. Louis, MO) slurry at a ratio of 40 µl CaSO₄ slurry to 1 ml alginate solution and allowed to gel between glass plates with a 1 mm spacer.

For experiments to examine the effects of hydrogel stiffness on cell proliferation, both high molecular weight and low molecular weight alginate were used. The ratio between CaSO₄ slurry and alginate was varied between 20 and 60 µl CaSO₄ slurry to 1 ml high molecular weight alginate solution and 20 to 40 µl CaSO₄ slurry to 1 ml low molecular weight alginate. Gel disks were punched using a 5 mm diameter puncher and incubated in DMEM for 36 hours, changing

media every 12 hours. The elastic modulus of the hydrogels were calculated from the slope of the compressive stress versus strain curve acquired using an MTS Insight Electromechanical Testing System. Cells were seeded on the disks at a density of 640 cells/mm² and incubated in complete growth media. Media was changed every 48 hours thereafter.

2.3.4 Three-dimensional cell culture in hydrogels

Low molecular weight alginate was used for three-dimensional (3D) cell culture studies. Gels without RGD peptides were made from unmodified low molecular weight alginate. Gels with RGD peptides were made by mixing unmodified low molecular weight alginate with G₄RGDASSKY-conjugated low molecular weight alginate in 9:1, 1:1, and 1:9 ratios. Cells were encapsulated in alginate gels at a density of 6×10^5 cells/ml by mixing equal volumes of the cell suspension and an alginate solution. The cell-alginate mixture was cross-linked with a CaSO₄ slurry at a ratio of 40 μ l CaSO₄ slurry to 1 ml cell-alginate mixture and allowed to gel between glass plates with a 1 mm spacer. 10 mm gel disks were punched and incubated in complete growth media. Media was changed after 24 hours and every 48 hours thereafter.

2.3.5 Analysis of stress fibers for 2D cultures

After culture of cells on the hydrogel surfaces for 5 days, cell-hydrogel constructs were fixed overnight in a solution of 4% formaldehyde (Sigma Aldrich), washed with phosphate buffer saline (PBS, Invitrogen), and permeabilized with a solution of 0.5% Triton X-100 (Sigma Aldrich) and 5% dry milk. Intracellular actin stress fibers were stained using Oregon Green 514 phalloidin (Invitrogen). Oregon Green 514 phalloidin was diluted in PBS to 5 units/ml, and 1 ml was used to stain each gel for 30 minutes. Gels were rinsed with 0.5% Triton X-100 and 5% dry

milk and then washed extensively in DMEM. The stained gels were visualized using a Leica TCS SP2 confocal system.

2.3.6 Cell proliferation assay for 2D cultures

Cell numbers on the 2D gels were analyzed on Days 1, 3, and 5. Four disks for each condition on each day were used for analysis. Four different micrographs were taken from random locations on each gel, and the total number of cells in each set of four micrographs was counted. The cell counts were normalized to those counted on Day 1.

2.3.7 Cell proliferation and viability assays for 3D cultures

Cell proliferation in the 3D gels was analyzed with MTS tetrazolium [3-(4,5-dimethylthiazol-2-yl)-5-(3-carboxymethoxyphenyl)-2-(4-sulfophenyl)-2H-tetrazolium, inner salt] (Promega Corporation, Madison, WI). Cells were treated with MTS, and viable cells were evaluated by the formation of a soluble formazan product. The amount of formazan produced was quantified with absorbance at 490nm, and the quantity of formazan measured was directly proportional to the number of viable cells in culture.

To visualize viable cells after 5 days of culture, the 3D cell-gel constructs were treated with tetrazolium MTT [3-(4,5-dimethylthiazolyl-2)-2, 5-diphenyltetrazolium bromide] (ATCC, Manassas, VA). Viable cells were evaluated by the formation of an insoluble dark purple formazan resulting from the reduction of the MTT reagent in mitochondria of viable cells. The treated cell-gel constructs were visualized using a Leica DMI 4000B microscope.

2.3.8 Immunohistochemistry analysis for 3D cultures

After 5 days of culture, the 3D cell-hydrogel constructs were fixed overnight in either 4% paraformaldehyde in PBS or 10% formaldehyde in PBS, both at pH 7.4. The hydrogels were then dehydrated in ascending percentages of ethanol, cleared in xylene, and embedded in low temperature paraffin. Sections were cut at a thickness of 5 μ m and affixed to pretreated glass slides. Slides were deparaffinized, hydrated, and boiled for 10 minutes in a microwave for antigen retrieval with 0.01 M citrate buffer, pH 6.0. Sections were incubated in the appropriate serum (10% normal goat or rabbit), followed by incubation with the primary antibody for 1 hour at 37 °C. Following a rinse with PBS, the sections were incubated with the appropriate biotin-conjugated secondary antibody at room temperature for 1 hour, rinsed again, and incubated with ABC solution (Vector Laboratories, Burlingame, CA) for 30 minutes. Sections were colorized with diaminobenzidine, counterstained with Mayer hematoxylin (Sigma Aldrich), dehydrated, and coverslipped. Negative control sections were treated in an identical manner but were incubated with PBS instead of the primary antibody. Antibodies used were anti-rabbit DDX4/MVH Primordial Germ Cell Marker (VASA) and anti-rat c-Kit (Caltag Laboratories, Burlingame, CA). Secondary antibodies used were a biotinylated goat anti-rabbit (DAKO USA, Carpinteria, CA) and a biotinylated goat anti-rat (Abcam, Cambridge, MA).

2.3.9 Statistical analysis

Statistical significance between two data populations was evaluated using an unpaired, two-tailed Student's t-test in Microsoft Excel. Differences were considered statistically significant for $p < 0.05$. Statistical significance among more than two data populations was

evaluated using a one-way analysis of variance (ANOVA) in Minitab. Data populations were considered statistically similar for $p > 0.1$

2.4 Results

2.4.1 Effects of RGD peptide densities and hydrogel stiffness on cell proliferation in 2D cultures

Hydrogels presenting different RGD peptide densities (N_{RGD}) were prepared by altering the ratio between alginate molecules modified with RGD peptides and unmodified alginate molecules from 1:9 to 9:1 to vary N_{RGD} from 6.2 to 56×10^7 RGD/mm². The RGD concentration on the surface of the hydrogel was calculated from the degree of substitution of RGD peptides and the ratio between modified and unmodified alginate assuming an alginate molecule occupies the same volume as a hard sphere with a radius equal to the radius of gyration of an alginate molecule. Changes in N_{RGD} had minimal effects on the hydrogel stiffness and swelling ratio.

The effects of N_{RGD} on the morphology and cytoskeleton of cells adhered to the gel surface were investigated by evaluating the formation of actin stress fibers. Increasing N_{RGD} enhanced the formation of intracellular actin stress fibers, which were remodeled upon cellular contractility (Figure 2.3). SSC colony formation was also enhanced with increasing N_{RGD} (Figure 2.4) while cell spreading was maximized at an intermediate N_{RGD} ; for single cells, the average projected cell areas at 6.2, 31, and 56×10^7 RGD/mm² were 84, 1500, and 510 μm^2 , respectively.

Cell proliferation on 2D hydrogel surfaces was significantly dependent on N_{RGD} . Each SSC seeded formed distinct colonies of daughter cells, and the number of cells in each colony increased with N_{RGD} during five days of cell culture, qualitatively indicating an enhancement in cell proliferation with N_{RGD} (Figure 2.5). A quantitative analysis of cell number over time also

confirmed that increasing cell adhesion sites promoted cell proliferation (Figure 2.6). The lowest N_{RGD} (6.2×10^7 RGD/mm²) showed a minimal increase in cell number, and the difference between normalized cell numbers for the lowest and highest N_{RGD} at Day 5 was statistically significant. The cell proliferation rate (k) was further quantified from Eq 1:

$$\frac{N}{N_0} = 2^{kt} \quad \text{Eq. 1}$$

where N represents the number of cells measured at a given time, N_0 represents the initial number of cells measured at Day 1, and t represents the cell culture period. The calculated k increased as N_{RGD} increased. The cell doubling time calculated from k decreased significantly as N_{RGD} was increased from 3.1×10^8 to 5.6×10^8 RGD/mm² (Figure 2.7).

In contrast, the stiffness of hydrogels played a minimal role in regulating cell proliferation. A quantitative analysis of cell number over time showed that at a constant N_{RGD} of 6.2×10^8 RGD/mm², changes in the elastic modulus did not significantly alter the extent of cell spreading, the number of cells per colony, or the overall cell numbers (Figure 2.8). The k values quantified using Eq 1 were statistically similar on hydrogels of different stiffness, indicating that k was roughly independent of the elastic modulus (Figure 2.9).

2.4.2 Effects of RGD peptide densities on cell proliferation in 3D cultures

Based on the results from cell proliferation on 2D gel surfaces, SSCs were encapsulated within four hydrogel formulations: unmodified alginate and alginate modified with RGD peptides at an N_{RGD} of 1.5, 7.3, and 13×10^{12} RGD/mm³ in order to confirm the critical roles of cell adhesion peptides on cell proliferation in 3D cultures. Low molecular weight alginate molecules were used for cell encapsulation in order to circumvent a loss of cell viability during

the encapsulation process (Kong et al, 2003). The elastic moduli of the gels were kept constant at 15 kPa since cell proliferation was not dependent on hydrogel stiffness in 2D cell culture.

Cell viability was evaluated by identifying viable cells with an MTT assay. The MTT reagent was reduced to an insoluble dark purple formazan in the mitochondria of living cells, thus allowing viable cells to be identified with a dark stain. Increasing N_{RGD} from 0 to 1.3×10^{13} RGD/mm³ increased the number of viable colonies; furthermore, cells encapsulated within hydrogels modified with RGD were mostly viable after five days in culture as compared with cells encapsulated within unmodified hydrogels (Figure 2.10). Increasing N_{RGD} from 0 to 1.3×10^{13} RGD/mm³ also resulted in an increase in the diameter of viable colonies (Figure 2.11).

Cell proliferation was evaluated with an MTS-based cell proliferation assay. Formazan produced by viable cells in the reduction of MTS was detected with absorbance at 490 nm. The measured absorbance, which was directly proportional to the number of viable cells, increased significantly with N_{RGD} (Figure 2.12). The cell proliferation rate (k) quantified using Eq 1 also increased with N_{RGD} (Figure 2.13). Gels with no RGD peptides resulted in negative k values, likely due to significant cell death.

The integrity of the SSCs cultured within hydrogels modified with RGD peptides was further examined. The expression of Vasa, a marker for undifferentiated SSCs, and c-kit, a marker for differentiating SSCs, were probed via immunostaining. Cells cultured within hydrogels modified with RGD peptides were positively stained for Vasa (Figure 2.14A and 2.14D) and negatively stained for c-kit (Figure 2.14B and 2.14E), indicating that the cells retained their undifferentiated germ cell properties. In the unmodified hydrogels, which did not contain RGD, cells did not proliferate and died after five days in culture; therefore, their phenotype could not be analyzed (data not shown). At an N_{RGD} of 1.5 and 7.3×10^{12} RGD/mm³,

cells proliferated but the size of the colonies remained small (Figure 2.14A-C). In comparison, colony sizes doubled with cells cultured at an N_{RGD} of 1.3×10^{13} RGD/mm³ (Figure 2.14D-F).

While N_{RGD} influenced the size of cell colonies, it did not affect Vasa or c-kit expression.

2.5 Discussion

This study uses an advanced 3D cell culture system, which mimics some of the biochemical and biomechanical components of the basement membrane, to support SSC proliferation. The culture system used in this study consisted of a bioactive hydrogel presenting cell adhesion molecules (RGD peptides) and was tested with varying cell adhesion sites and stiffness. Interestingly, SSC proliferation could be regulated both in 2D and 3D cell cultures solely by altering hydrogel properties, without the addition of GDNF or other exogenous soluble factors.

The proliferation rates of SSCs and adhesion to the gel matrix were significantly dependent on the density of RGD peptides. In 2D cultures, the number of RGD peptides contributed to increasing the number of intracellular stress fibers but did not control the extent of SSC spreading. In 3D cultures, the number of RGD peptides contributed to the formation of viable cell colonies. It is likely that an increase in RGD peptide density led to an increase in the number of bonds between cellular integrins and RGD peptides, as previously examined (Kong et al, 2006). This increase in bond number promoted focal adhesion formation at the cell adhesion sites and subsequent intracellular stress fiber formation. It has been reported that this intracellular cytoskeletal reorganization influences the signaling pathways for cell division in both 2D and 3D cell culture (Margadant et al, 2007). SSCs prominently express $\alpha_6\beta_1$ integrins, which are known to bind to laminin in the basement membrane, and laminin is known to be

important in the maintenance of stem cells in general (Shinohara et al, 1999). The fact that RGD modulates SSC proliferation *in vitro* implies either that the RGD on the α chain of laminin is important for SSC biology, or/and that other basement membrane proteins containing RGD play a role in SSC biology (Tashiro et al, 1991).

In contrast, SSC proliferation was not influenced by mechanical stiffness of the hydrogels. Previous studies have demonstrated that the mechanical stiffness of hydrogels plays a critical role in regulating the proliferation of pre-osteoblast cells but a minimal role in regulating the proliferation of bone marrow-derived stem cells (Hsiong et al, 2007). Previous studies have also demonstrated that mechanical stiffness plays a role in regulating the differentiation of both stem and precursor cells (Engler et al, 2006). The lack of dependency of SSC proliferation on hydrogel stiffness is thus similar to the response of bone marrow-derived stem cells. This result may be due to the lack of intrinsic factors in SSCs which respond to mechanical stress, in comparison to more differentiated cells or cells belonging to other lineages, such as pre-osteoblasts.

Overall, this study demonstrates that a bioactive hydrogel modified with synthetic oligopeptides can be highly useful in controlling SSC proliferation in both 2D and 3D cell culture by mimicking some of the biochemical properties of the basement membrane underlying the seminiferous epithelium. In addition, the results of this study identified a key ECM variable that might regulate the proliferation of primary SSCs in the natural stem cell niche. The differentiation of primary SSCs into specific lineages may be regulated with the appropriate soluble factors for cells cultured within the hydrogel or for cells isolated from the hydrogel. Therefore, the hydrogel system used in this study presents strong potential for use as a primary SSC transplantation vehicle in various cell-based therapies. In addition, the crucial role of natural

stem cell niches in regulating stem cell activities can be further clarified using this synthetic hydrogel system. Therefore, the results of this study would be broadly applicable to understanding the interactions between various stem cells and their microenvironments and ultimately controlling the diverse activities of a broad array of stem cells.

2.6 References

1. Boontheekul T, Hill EE, Kong HJ, Mooney DJ. Regulating myoblast phenotype through controlled gel stiffness and degradation. *Tissue Engineering* 13, 1431, 2007.
2. Braydich-Stolle L, Kostereva N, Dym M, Hofmann MC. Role of Src family kinases and N-Myc in spermatogonial stem cell proliferation. *Developmental Biology* 304, 34, 2007.
3. Candiello J, Balasubramani M, Schreiber EM, Cole GJ, Mayer U, Halfter W, Lin H. Biomechanical properties of native basement membranes. *FEBS Journal*, 274, 2897, 2007.
4. Discher DE, Janmey P, Wang YL. Tissue cells feel and respond to the stiffness of their substrate. *Science* 310, 1139, 2005.
5. Engler AJ, Sen S, Sweeney HL, Discher DE. Matrix elasticity directs stem cell lineage specification. *Cell* 126, 677, 2006.
6. Erickson AC and Couchman JR. Still more complexity in mammalian basement membranes. *Journal of Histochemistry and Cytochemistry* 48, 1291, 2000.
7. Gardner JM and Hynes RO. Interaction of fibronectin with its receptor on platelets. *Cell* 42, 439, 1985.
8. Geiger B, Bershadsky A, Pankov R, Yamada KM. Transmembrane crosstalk between the extracellular matrix and the cytoskeleton. *Nature Reviews Molecular Cell Biology* 2, 793, 2001.
9. Giancotti FG and Ruoslahti E. Integrin signaling. *Science* 285, 1028, 1999.
10. Griffith LG, and Swartz MA. Capturing complex 3D tissue physiology in vitro. *Nature Reviews Molecular Cell Biology* 7, 211, 2006.
11. Guan K, Nayernia K, Maier L, Wagner S, Dressel R, Lee J, Nolte J, Wolf F, Li M, Engel W, Hasenfuss G. Pluripotency of spermatogonial stem cells from adult mouse testis. *Nature* 440, 1199, 2006.
12. Gumbiner BM. Cell adhesion: the molecular basis of tissue architecture and morphogenesis. *Cell* 84, 345, 1996.
13. He Z, Jiang J, Kokkinaki M, Golestaneh N, Hofmann MC, Dym M. GDNF up-regulates c-fos transcription via the Ras/ERK1/2 pathway to promote mouse spermatogonial stem cell proliferation. *Stem Cells* 26, 266, 2008.
14. Hofmann M, Braydich-Stolle L, Dettin L, Johnson E, Dym M. immortalization of mouse germ line stem cells. *Stem Cells* 23, 200, 2005.

15. Hsiong SX, Carampin P, Kong HJ, Lee K, Mooney DJ. Differentiation stage alters matrix control of stem cells. *Journal of Biomedical Materials Research A* 85A, 145, 2008.
16. Kanatsu-Shinohara M, Inoue K, Lee J, Yoshimoto M, Ogonuki N, Miki H, Baba S, Kato T, Kazuki Y, Toyokuni S, Toyoshima M, Niwa O, Oshimura M, Heike T, Nakahata T, Ishino F, Ogura A, Shinohara T. Generation of pluripotent stem cells from neonatal mouse testis. *Cell* 119, 1001, 2004.
17. Kanatsu-Shinohara MH, Inoue K, Ogonuki N, Toyokuni S, Ogura A, Shinohara T. Long-term culture of mouse male germline stem cells under serum-or feeder-free conditions. *Biology of Reproduction* 72, 985, 2005.
18. Kong HJ, Boonthekul T, Mooney DJ. Quantifying the relation between adhesion ligand-receptor bond formation and cell phenotype. *Proceedings of the National Academy of Sciences USA* 103, 18534, 2006.
19. Kong HJ, Hsiong S, Mooney DJ. Nanoscale cell adhesion ligand presentation regulates non-viral gene delivery and expression. *Nano Letters* 7, 161, 2007.
20. Kong HJ, Lee KY, Mooney DJ. Decoupling the dependence of rheological/mechanical properties of hydrogels from solids concentration. *Polymer*, 43, 6239, 2002.
21. Kong HJ, Polte TR, Alsberg E, Mooney DJ. FRET measurements of cell-traction forces and nano-scale clustering of adhesion ligands varied by substrate stiffness. *Proceedings of the National Academy of Sciences USA* 102, 4300, 2005.
22. Kong HJ, Smith MK, Mooney DJ. Designing alginate hydrogels to maintain viability of immobilized cells. *Biomaterials* 24, 4023, 2003.
23. Kubota H, Avarbock MR, Brinster RL. Growth factors essential for self-renewal and expansion of mouse spermatogonial stem cells. *Proceedings of the National Academy of Sciences USA* 101, 16489, 2004.
24. Lee KY. Alsberg E, Hsiong S, Comisar W, Linderman J, Ziff R, Mooney DJ. Nanoscale adhesion ligand organization regulates osteoblast proliferation and differentiation. *Nano Letters* 4, 1501, 2004.
25. Lee KY and Mooney DJ. Hydrogels for tissue engineering. *Chemical Reviews* 101, 1869, 2001.
26. Li L and Xie T. Stem cell niche: structure and function. *Annual Review of Cell and Developmental Biology* 21, 605, 2005.
27. Lu X, Pandit A, Kassab GS. Biaxial incremental homoelastic moduli of coronary artery: two-layer model. *American Journal of Physiology - Heart and Circulatory Physiology*, 287, H1663, 2004.

28. Lutolf MP and Hubbell JA. Synthetic biomaterials as instructive extracellular microenvironments for morphogenesis in tissue engineering. *Nature Biotechnology* 23, 47, 2005.
29. Margadant C, van Opstal A, Boonstra J. Focal adhesion signaling and actin stress fibers and dispensable for progression through the ongoing cell cycle. *Journal of Cell Science* 120, 66, 2007.
30. McMillan J, Akiyama M, Shimizu H. Epidermal basement membrane zone components: ultrastructural distribution and molecular interactions. *Journal of Dermatological Science* 31, 169, 2003.
31. Moore K and Lemischka I. Stem cells and their niches. *Science* 311, 1880, 2006.
32. Pierschbacher M and Ruoslahti E. Cell attachment activity of fibronectin can be duplicated by small synthetic fragments of the molecule. *Nature* 309, 30, 1984.
33. Rowley JA and Mooney DJ. Alginate type and RGD density control myoblast phenotype. *Journal of Biomedical Materials Research* 60, 217, 2002.
34. Rowley JA, Madlambayan G, Mooney DJ. Alginate hydrogels as synthetic extracellular matrix materials. *Biomaterials* 20, 45, 1999.
35. Schofield R. The relationship between the spleen colony-forming cell and the hemopoietic stem cell. *Blood Cells* 4, 7, 1978.
36. Shinohara T, Avarbock M, Brinster R. beta1- and alpha6-integrin are surface markers on mouse spermatogonial stem cells. *Proceedings of the National Academy of Sciences USA* 96, 5504, 1999.
37. Smetana K. Cell biology of hydrogels. *Biomaterials* 14, 1046, 1993.
38. Stevens MM and George JH. Exploring and engineering the cell surface interface. *Science* 310, 1135, 2005.
39. Tashiro KI, Sephel GC, Grestorex D, Sasaki M, Shirashi N, Martin GR, Kleinman HK, Yamada Y. The RGD containing site of the mouse laminin A chain is active for cell attachment, spreading, migration and neurite outgrowth. *Journal of Cellular Physiology* 146, 451, 1991.
40. Watt F and Hogan B. Out of Eden: stem cells and their niches. *Science* 287, 1427, 2000.
41. Yoshida S, Sukeno M, Nabeshima Y. A vasculature-associated niche for undifferentiated spermatogonia in the mouse testis. *Science* 317, 1722, 2007.

2.7 Figures

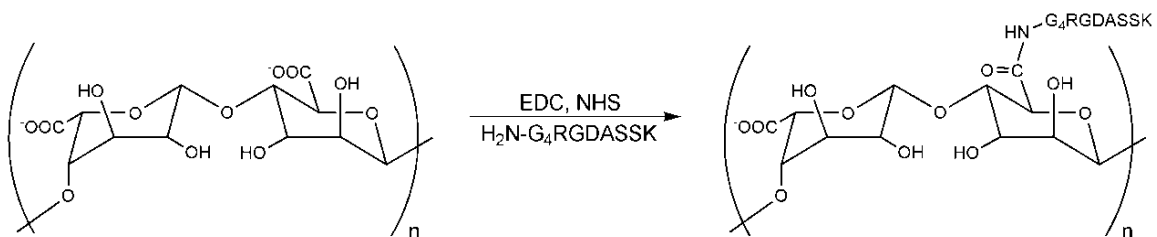


Figure 2.1 RGD-alginate synthesis. Arg-Gly-Asp (RGD) peptides were conjugated to alginate using carbodiimide chemistry.

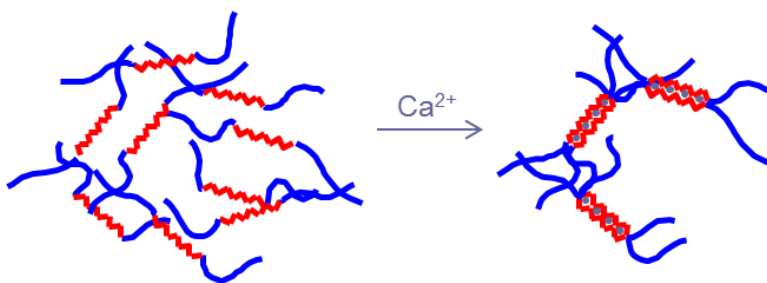
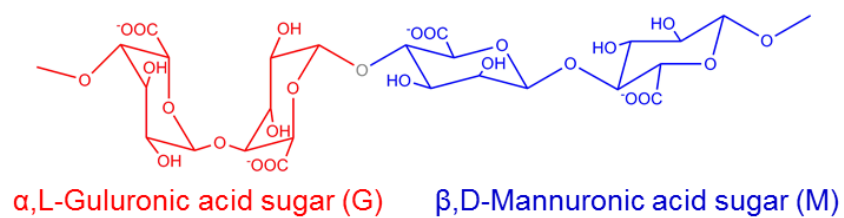


Figure 2.2 Alginate hydrogel formation. Alginate solutions were ionically cross-linked with a calcium sulfate slurry. Multivalent cations, such as Ca^{2+} , are known to cross-link the G blocks in alginate.

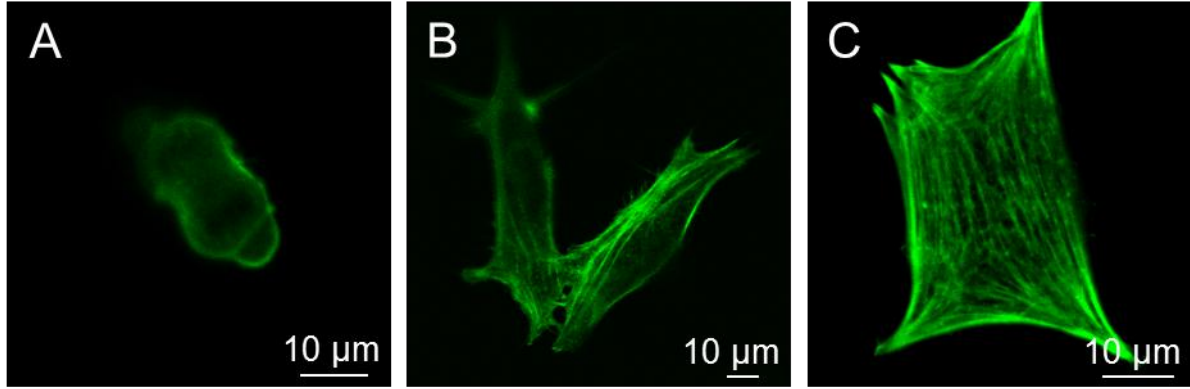


Figure 2.3 Effect of N_{RGD} on SSC actin stress fiber formation in 2D. The overall density of RGD peptides immobilized on hydrogel surfaces (N_{RGD}) influenced cellular contractility. Intracellular actin stress fiber formation was visibly enhanced as N_{RGD} was increased. (A), (B), and (C) represent C18-4 cells attached to gels presenting N_{RGD} of 6.2 , 31 , and 56×10^7 RGD/mm², respectively. Green fluorescence in microphotographs represents actin fibers stained with Oregon Green 514 phalloidin. Images were captured after five days of culture.

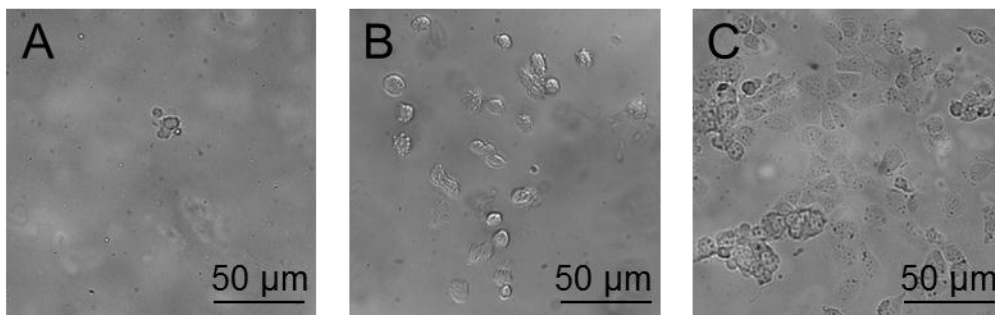


Figure 2.4 Effect of N_{RGD} on SSC colony formation in 2D. SSC colony formation on 2D surfaces was enhanced with increasing N_{RGD} . (A), (B), and (C) represent C18-4 cells attached to gels presenting N_{RGD} of 6.2 , 31 , and 56×10^7 RGD/mm², respectively.

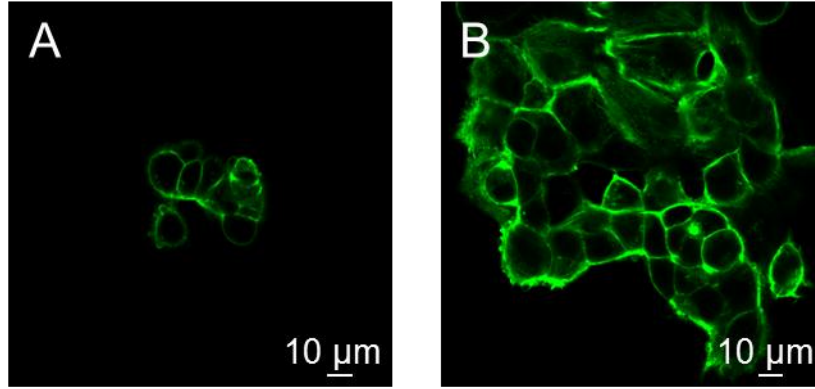


Figure 2.5 Effect of N_{RGD} on SSC colony size in 2D. The overall density of RGD peptides immobilized on hydrogel surfaces (N_{RGD}) influenced C18-4 colony formation. The number of cells per colony increased as N_{RGD} was increased from 31×10^7 RGD/mm² (A) to 56×10^7 RGD/mm² (B). Green fluorescence in microphotographs represents actin fibers stained with Oregon Green 514 phalloidin. Images were captured after five days of culture.

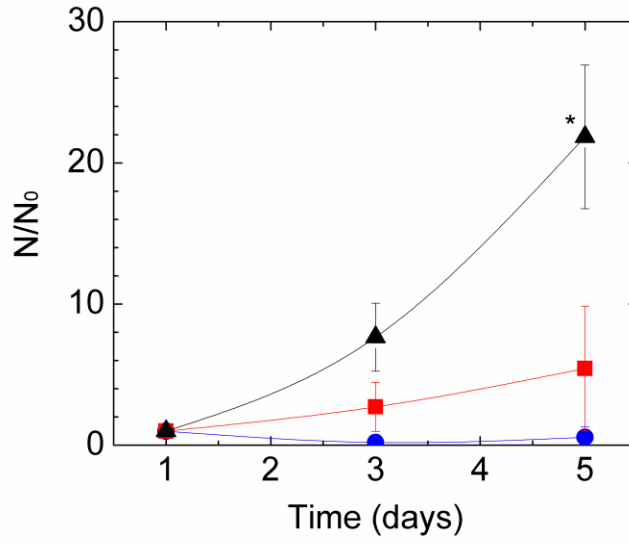


Figure 2.6 Effect of N_{RGD} on SSC cell number over time in 2D. Cell proliferation on 2D hydrogel surfaces was regulated by the overall density of RGD peptides immobilized on hydrogel surfaces (N_{RGD}). The increase in cell number (N) over time was accelerated with N_{RGD} . N and N_0 represent the cell number and the cell number measured at Day 1, respectively. ●, ■, and ▲ represent N_{RGD} of 6.2 , 31 , and 56×10^7 RGD/mm², respectively. Differences between N/N_0 at Day 5 for the highest and lowest N_{RGD} were statistically significant (* $p < 0.05$).

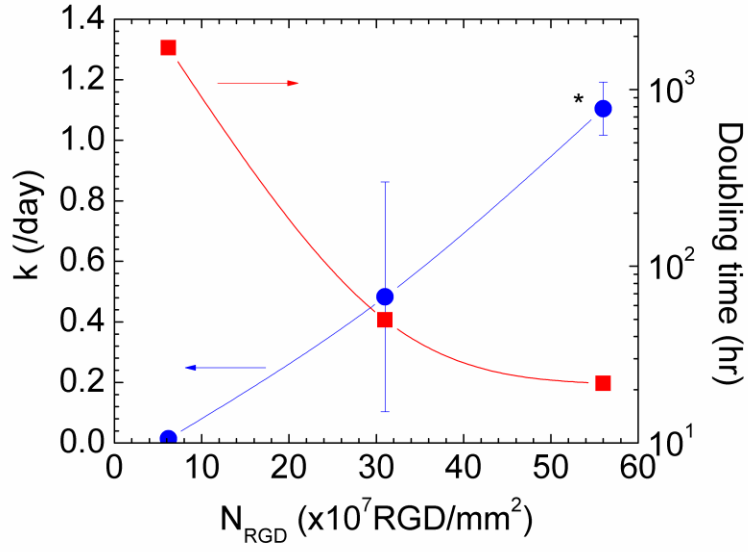


Figure 2.7 Effects of N_{RGD} on proliferation rate of SSCs in 2D. The cell proliferation rate (k) increased with N_{RGD} . • and ■ represent k and doubling time, respectively. Differences between the calculated k values at the highest and lowest N_{RGD} were statistically significant (* $p < 0.05$). Values represent the mean and standard deviation from four independent measurements.

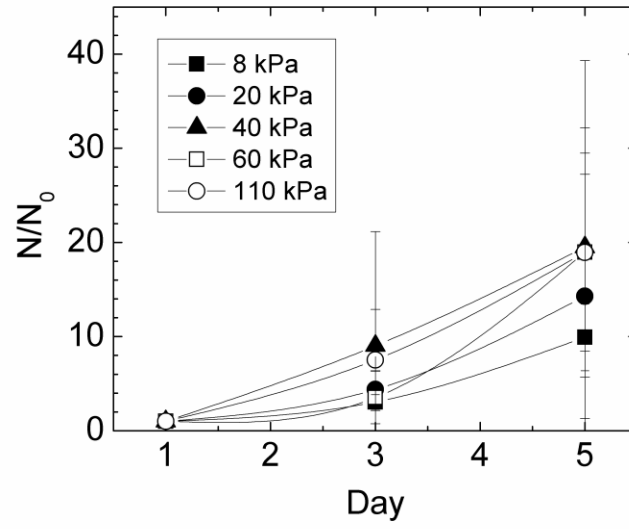


Figure 2.8 Effects of substrate stiffness on SSC cell number over time in 2D. Cell proliferation on 2D hydrogel surfaces was roughly independent of the elastic modulus of the hydrogel. N_{RGD} was kept constant at 6.2×10^8 RGD/mm² while the elastic modulus was varied from 8 kPa to 110 kPa. N and N_0 represent the cell number and the cell number measured at Day 1, respectively. ■, ●, ▲, □, and ○ represent gels with elastic moduli of 8, 20, 40, 60, and 110 kPa, respectively.

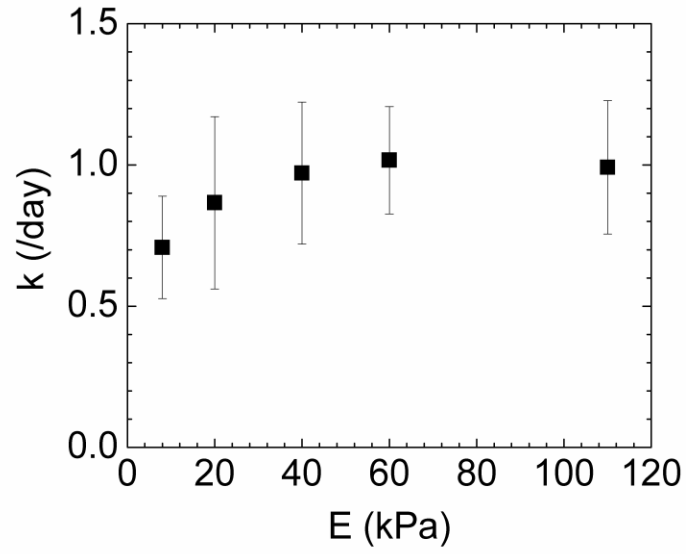


Figure 2.9 Effects of substrate stiffness on SSC proliferation. The stiffness of hydrogels did not significantly influence C18-4 cell proliferation. Cell proliferation rate (k) on 2D hydrogel surfaces, calculated from the increase in cell number over time, was roughly independent of the elastic modulus of the hydrogel (E). N_{RGD} was kept constant at 6.2×10^8 RGD/mm². The calculated k values were statistically similar on gels of different stiffness, as determined with ANOVA. Values represent the mean and standard deviation from four independent measurements.

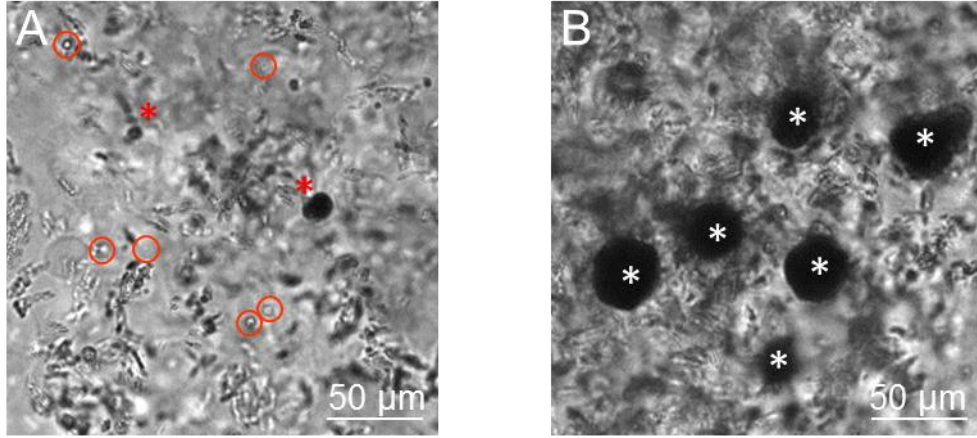


Figure 2.10 Effect of N_{RGD} on SSC colony formation in 3D. The overall density of RGD peptides (N_{RGD}) influenced C18-4 colony formation in 3D cultures. Increasing N_{RGD} from 0 (A) to 1.3×10^{13} RGD/mm³ (B) within a 3D hydrogel matrix increased SSC colony formation. The number of viable cells positively stained with an MTT assay also increased with N_{RGD} . In (A) and (B), viable SSC colonies positively stained with MTT are represented with asterisk (*), while nonviable cells, unstained with MTT, are circled.

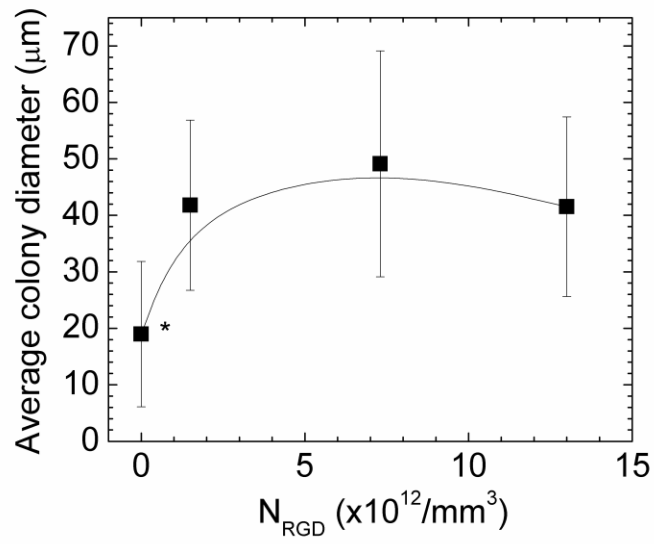


Figure 2.11 Effect of N_{RGD} on SSC colony size in 3D. The overall density of RGD peptides (N_{RGD}) influenced C18-4 colony formation in 3D cultures. The average diameter of viable cell colonies increased with increasing N_{RGD} . Differences between average cell colony diameters in gels without RGD as compared to gels presenting RGD were statistically significant (* $p < 0.05$).

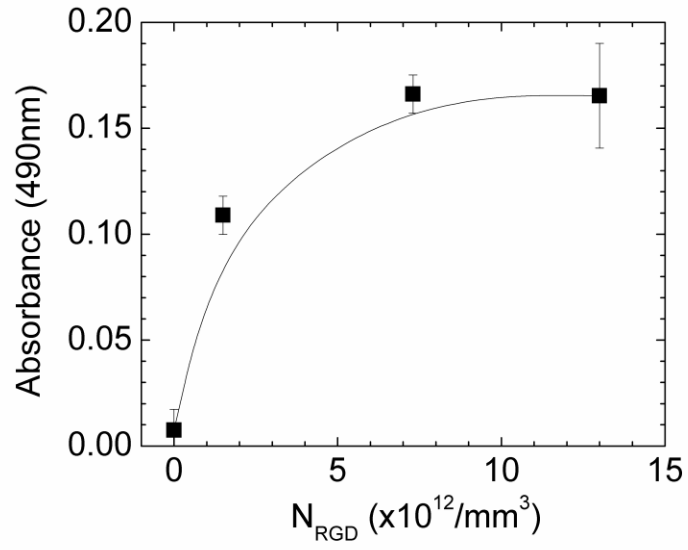


Figure 2.12 Effect of N_{RGD} on cell viability in 3D. Cell viability in 3D hydrogel cultures on Day 5 increased with increasing RGD density. The absorbance measured at 490nm, in accordance with an MTS-based proliferation assay, is proportional to the number of viable cells. N_{RGD} was varied from 0 to 1.3×10^{13} RGD/mm³.

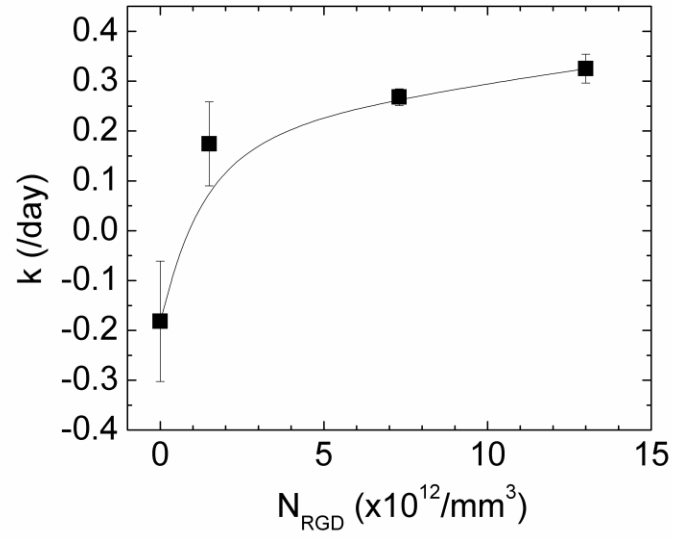


Figure 2.13 Effect of N_{RGD} on SSC proliferation in 3D. The cell proliferation rate (k) of C18-4 cells cultured in 3D increased with increasing N_{RGD} . Differences between calculated k values were statistically significant on gels with different N_{RGD} , as determined with ANOVA. The elastic moduli of the hydrogels were kept constant at 15 kPa.

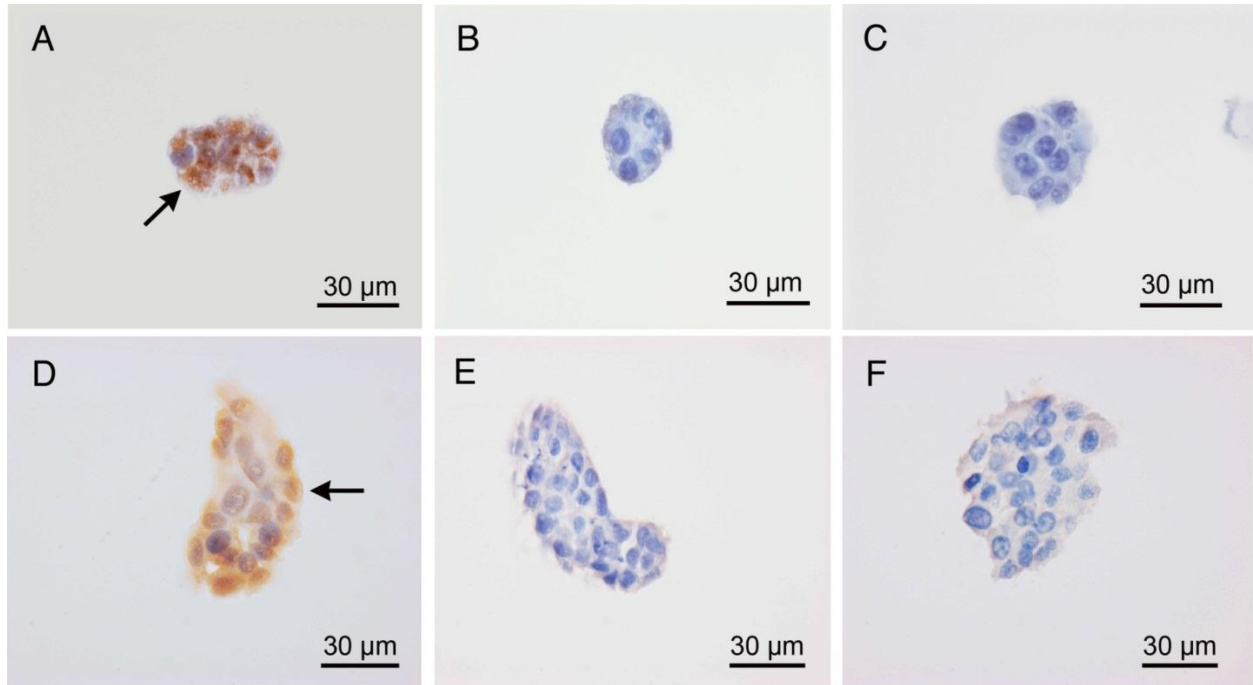


Figure 2.14 Immunocytochemistry analysis of SSC colonies in 3D. Cells cultured in 3D hydrogels expressed Vasa but did not express c-Kit. N_{RGD} was varied from 1.5×10^{12} RGD/mm³ (A–C) to 1.3×10^{13} RGD/mm³ (D–F). Cells expressed Vasa at all N_{RGD} , as indicated with arrows (A and D). Cells did not express the c-Kit protein at any N_{RGD} (B and E). (C) and (F) represent negative controls, colonies stained without primary antibodies.

CHAPTER 3: INTERPLAY OF CELL ADHESION MATRIX STIFFNESS AND CELL TYPE FOR NON-VIRAL GENE DELIVERY*

3.1 Introduction

Non-viral gene delivery has the potential to treat a wide array of diseases through the transfer of genetic material while circumventing safety concerns associated with viral vectors (Luo and Saltzman, 2000; Glover et al, 2005; Pack et al, 2005). To facilitate entry to target cells, therapeutic genes are often packaged with delivery vectors, such as polycations, lipids, dendrimers, and virus-mimicking constructs (Putnam, 2006; Mintzer and Simanek, 2009). The resulting polyplexes can be administered directly to the target tissue to induce exogenous expression in host cells or loaded into a provisional matrix for tissue regeneration (Storrie and Mooney, 2006; De Laporte and Shea 2007; O'Rourke et al, 2010). While non-viral gene delivery holds much promise and has demonstrated impressive results, it still suffers from limited and inconsistent expression *in vivo* (Pack et al, 2005; Pouton and Seymour, 2001; Wiethoff and Middaugh 2003; rose et al, 2012).

Several *in vitro* studies have recently reported that gene delivery to cells cultured on a synthetic extracellular matrix (ECM) can be regulated with chemical and mechanical properties of the matrix. For example, gene transfection efficiency has been regulated by matrix stiffness (Kong et al, 2005) and cell adhesion domains (Kong et al, 2007; Dhaliwal et al, 2012) for cells cultured on synthetic substrates. In these studies, the effects of matrix properties on gene delivery were attributed to changes in cellular proliferation rate affecting gene uptake as well as intracellular activities affecting gene expression.

* This chapter contains work accepted for publication in *Acta Biomaterialia* and is reprinted here with the permission of Elsevier.

Recent studies have also reported that the extent to which ECM properties influence cellular activities varies among cell types (Yeung et al, 2005; Georges and Janmey, 2005; Discher et al, 2005). For example, the proliferation rate of bone precursor cells was shown to increase with increasing matrix stiffness while the proliferation rate of bone marrow stromal cells was less dependent on matrix stiffness (Hsiong et al, 2008). Similarly, the role of matrix properties in gene delivery may be mediated by cell type, but this has not yet been systematically examined to date.

3.2 Objective and scope

In this study, we hypothesized that the stiffness of a cell adhesion matrix regulates non-viral gene delivery to various extents for different cell types due to changes in gene uptake and intracellular processes affecting gene expression. We examined this hypothesis by evaluating the delivery of plasmid DNA (pDNA) to NIH3T3 fibroblasts, D1 bone marrow stromal cells, and C2C12 myoblasts cultured independently on fibronectin-conjugated poly(ethylene glycol) hydrogels tuned to present various elastic moduli. These three cell types can be found in skeletal muscle tissue, which is a common administration site for genes in preclinical and clinical settings. The elastic moduli of the hydrogels were varied from 10 to 670 kPa, which encompasses the stiffness of skeletal muscle and collagenous bone (Engler et al, 2006). pDNA encoding bone morphogenetic protein (BMP)-2, which has been used in tissue regeneration therapies (Lieberman et al, 1999; Kirker-Head 2000), was used as a model gene. The uptake of pDNA and resulting BMP-2 expression were quantified to examine the effects of matrix stiffness and cell type on gene transfection efficiency. In parallel, cell proliferation, projected cell area,

and nuclear aspect ratio were examined to elucidate the underlying mechanism by which matrix stiffness influences non-viral gene delivery for the three cell types in this study.

3.3 Materials and methods

3.3.1 Poly(ethylene glycol) diacrylate hydrogel preparation

Poly(ethylene glycol) (MW = 508 g/mol) diacrylate (PEGDA; Polysciences, Inc., Warrington, PA) hydrogels were prepared by cross-linking PEGDA molecules dissolved in deionized water. The polymer concentration of the pre-gel solution was varied from 5 to 20% (v/v) to control hydrogel stiffness. The pre-gel solution was mixed with ammonium persulfate (Sigma Aldrich, St. Louis, MO) and N,N,N',N'-tetramethylethylenediamine (TEMED, Sigma Aldrich). The concentrations of ammonium persulfate and TEMED in each sample were kept constant at 0.25% (w/v) and 2.5% (v/v), respectively. The pre-gel solution was allowed to gel for ten minutes in 48-well tissue culture plates or between glass plates with a 1 mm spacer. The resulting hydrogel surface was further modified by chemically linking fibronectin to the surface with the use of sulfosuccinimidyl 6-(4'-azido-2'-nitrophenylamino) hexanoate (Sulfo-SANPAH, Thermo Fisher Scientific, Rockford, IL). The surface of the gel was covered with a solution of 5 mM sulfo-SANPAH in 50 mM HEPES (Fisher Scientific, Pittsburgh, PA) and exposed to ultraviolet light using a CHIPhERASER Model 20 (Jelight Company Inc) for 10 minutes. This exposure was then repeated with fresh Sulfo-SANPAH solution. The gels were washed in 50 mM HEPES to remove any unbound Sulfo-SANPAH and incubated with 50 µg/ml fibronectin (Sigma Aldrich) overnight at 4 °C to allow the fibronectin to react with the Sulfo-SANPAH bound to the hydrogel surface. The gels were washed and incubated in Dulbecco's

modified Eagle's medium for three days (DMEM; Invitrogen, Carlsbad, CA) to remove any excess soluble chemicals.

The compressive elastic moduli of PEGDA hydrogels were measured using a mechanical tester (Insight, MTS Systems, Eden Prairie, MN). PEGDA hydrogels were prepared as described above between glass plates with a 1 mm spacer. PEGDA hydrogel disks were punched and incubated in deionized water for one hour. These disks were then compressed at a rate of 1 mm/min, and the elastic moduli of the disks were calculated from the linear slope of the stress versus strain curve for the first 10% strain. The swelling ratio of the hydrogels was quantified from the mass ratio of hydrated disks to dried disks.

3.3.2 Cell culture on hydrogels of varied stiffness

NIH3T3 fibroblasts (ATCC, Manassas, VA), D1 bone marrow stromal cells (ATCC), and C2C12 myoblasts (ATCC) were cultured in Dulbecco's modified Eagle's medium (DMEM; Invitrogen, Carlsbad, CA) supplemented with 10% fetal bovine serum (FBS; Invitrogen) and 100 units/mL penicillin-streptomycin (Invitrogen) at 37°C in a 5% CO₂ incubator. For gene delivery experiments, cells were seeded on hydrogel substrates at a density of 300 cells/mm².

3.3.3 Analysis of cell proliferation

Cell proliferation on the hydrogel substrates was examined by quantifying the increase in cellular metabolic activity over four days. Cells cultured on PEGDA hydrogels were treated with MTS tetrazolium (Promega, Madison, WI) one and four days after seeding. Cellular metabolic activity was evaluated by the formation of a soluble formazan product, detectable with absorbance at 490 nm. The absorbance values, which are linearly proportional to the number of

viable cells, were measured using a Synergy HT plate reader (BioTek, Winooski, VT). The background absorbance for the assay was subtracted from the absorbance readings for each sample. To evaluate cell proliferation over the four day culture period, absorbance values measured on Day 4 were normalized to those measured on Day 1.

3.3.4 Delivery of pDNA encoding BMP-2 and evaluation of BMP-2 expression

pDNA encoding BMP-2 was first obtained from Christopher Evans at Brigham and Women's Hospital (Harvard University) and expanded by Aldevron (Fargo, ND). The pDNA was condensed with linear poly(ethylene imine) (MW = 25,000 g/mol) (PEI; Polysciences, Inc.). In brief, pDNA and PEI solutions were made in phosphate buffered saline (PBS, Invitrogen) and mixed at an N/P ratio of 9. The N/P ratio represents the molar ratio between the amine groups on PEI and the phosphate groups on pDNA. The resulting polyplex solution contained 50 µg/ml pDNA.

Cells were seeded on fibronectin-conjugated PEGDA hydrogels in complete growth media. 24 hours after seeding, 50 µl of polyplex solution was administered to the cells in 500 µl complete growth media. Cells remained exposed to the polyplex solution for 3 days without media changes after which the cell culture media was collected and BMP-2 expression was evaluated using a BMP-2 enzyme-linked immunosorbant assay (ELISA, R&D Systems, Minneapolis, MN). In brief, the media was incubated on a microplate coated with a monoclonal antibody specific for BMP-2. Any BMP-2 present in the media bound to the immobilized antibody and was detected with an enzyme-linked monoclonal antibody specific for BMP-2. Upon addition of a substrate solution, the absorbance of the final solution at 450 nm and 540 nm were measured using a Synergy HT plate reader. The absorbance at 540 nm was subtracted from

the absorbance at 450 nm, and the amount of BMP-2 detected was calculated from a calibration curve established using BMP-2 standards. The detected amount of BMP-2, measured in ng, was then normalized to cellular metabolic activity, which was measured with an MTS assay.

For certain experiments, cells were transfected with pDNA encoding BMP-2 via electroporation with the Neon Transfection System (Invitrogen). With the Neon Transfection System 10 µl Kit, cells were suspended in Buffer R at a density of 5×10^6 cells/ml. pDNA encoding BMP-2 was added to the cell suspension at 50 µg/ml, and 10 µl of the resulting solution was aspirated into each Neon Transfection Tip. The electroporation conditions were as follows: 2 pulses of 1400 V for 20 ms for fibroblasts, 3 pulses of 1600 V for 10 ms for BMSCs, and 3 pulses of 1650 V for 10 ms for myoblasts. After electroporation, the contents of the tip were ejected into complete growth media without antibiotics, as directed by the manufacturer of the electroporation unit due to negative effects of antibiotics on the viability of electroporated cells, and plated on hydrogels with varied elastic moduli, following the same procedure as described above. After 3 days, BMP-2 expression was evaluated with an BMP-2 immunoassay and normalized to cellular metabolic activity, as described above.

3.3.5 Analysis of cellular uptake of fluorescently-labeled pDNA

For experiments to quantify the cellular uptake of pDNA, pDNA encoding BMP-2 was labeled with YOYO-1 (Invitrogen). In brief, 200 µg of pDNA were incubated with 0.5 µl of a 1 mM solution of YOYO-1 for 1 hour at room temperature. For experiments to image pDNA uptake, pDNA encoding BMP-2 was labeled with ChromaTide Alexa Fluor 488-5-dUTP (Invitrogen) following the Nick Translation protocol from Invitrogen. In brief, pDNA and ChromaTide Alexa Fluor 488-5-dUTP were incubated for two hours at 15 °C in a buffer

containing Tris-HCl (Sigma Aldrich), magnesium chloride (Sigma Aldrich), and nuclease-free BSA (Sigma Aldrich) along with DTT (Gold Biotechnology, St. Louis, MO), a mixture of dGTP, dATP, dCTP, and dTTP (Invitrogen), DNase I (Sigma Aldrich), and DNA polymerase I (Invitrogen). The resulting labeled pDNA was purified with a QIAquick PCR Purification Kit (QIAGEN, Valencia, CA), and the concentration of pDNA in the purified solution was quantified with 4',6-diamidino-2-phenylindole (DAPI, Invitrogen).

To examine the uptake of fluorescently-labeled pDNA, polyplexes were prepared by mixing fluorescent pDNA with linear PEI solution, as described above. Cells were cultured on fibronectin-conjugated PEGDA hydrogels and exposed to polyplexes for 24 hours. The cells were then washed, fixed in a formaldehyde solution, and imaged using a Leica DMI 400B microscope. The fluorescent intensity of the images was quantified with integrated density using ImageJ software (National Institutes of Health) and normalized to cell number. For higher magnification images, cells were imaged using a Zeiss LSM 700 confocal microscope.

3.3.6 Analysis of projected cell area and nuclear aspect ratio

The projected area and nuclear aspect ratio of cells cultured on hydrogels of varied stiffness were analyzed from microscopy images. Cells were cultured on fibronectin-conjugated PEGDA hydrogels of varied stiffness for 24 hours and fixed in a formaldehyde solution for staining and imaging. The cell nuclei were stained with 4',6-diamidino-2-phenylindole (DAPI, Invitrogen), and the cell membranes were stained with CellMask Deep Red Plasma Membrane Stain (Invitrogen). The stained cells were then imaged using a Zeiss LSM 700 confocal microscope. The projected cell area was measured using ImageJ software. The nuclear aspect

ratio was calculated from the lengths of the major and minor axes of nuclei as measured using ImageJ software:

$$\text{nuclear aspect ratio} = \frac{\text{length of major axis of nucleus}}{\text{length of minor axis of nucleus}}$$

Twenty cells were randomly selected from each condition for quantified analysis of projected area and nuclear aspect ratio.

3.3.7 Statistical analysis

Statistical significance between two data populations was evaluated using an unpaired, two-tailed Student's t-test in Microsoft Excel. Differences were considered statistically significant for $p < 0.05$ and statistically similar for $p > 0.1$.

3.4 Results

3.4.1 Characterization of poly(ethylene glycol) diacrylate hydrogels

PEGDA hydrogels of tunable stiffness were prepared by cross-linking solutions with varying PEGDA concentrations. As the PEGDA concentrations in the pre-gel solutions were increased from 5 to 20%, the elastic moduli of the resulting hydrogels (E_{gel}) increased from 10 to 670 kPa while the swelling ratios decreased from 16 to 4.5 (Figure 3.1). The hydrogels exhibited minimal changes in elastic moduli and swelling ratios during seven days of incubation in cell culture media. Fibronectin was chemically conjugated to the hydrogel surface using a bi-functional linker, Sulfo-SANPAH, which has been previously reported to yield consistent protein conjugations independent of changes in hydrogel elastic modulus (Khatiwala et al, 2006).

3.4.2 Cellular uptake of pDNA encoding BMP-2 and resulting BMP-2 expression as mediated by matrix stiffness

Cellular uptake of pDNA encoding BMP-2 and subsequent BMP-2 expression were evaluated for fibroblasts, bone marrow stromal cells (BMSCs), and myoblasts cultured on fibronectin-conjugated poly(ethylene glycol diacrylate) (PEGDA) hydrogels with varied elastic moduli. Polyplexes prepared by condensing fluorescently labeled pDNA with linear PEI were delivered to fibroblasts (Figure 3.2a-c), BMSCs (Figure 3.2d-f), and myoblasts (Figure 3.2g-i) cultured on hydrogels with varying E_{gel} . The cellular uptake of fluorescently-labeled polyplexes, as quantified with integrated density, was found to increase with increasing E_{gel} for all three cell types. The increase in cellular uptake of pDNA was most significant for fibroblasts while the cellular uptake of pDNA for myoblasts exhibited minimal dependency on substrate stiffness (Figure 3.3). No fluorescence was observed from cells treated with unlabeled pDNA.

Next, exogenous BMP-2 expression was evaluated by measuring the amount of BMP-2 secreted in the cell culture media. The total amount of BMP-2 expressed, measured in picograms, increased with increasing E_{gel} for all three cell types, and expression levels from fibroblasts were highest on all E_{gel} when compared with expression levels from BMSCs and myoblasts (Figure 3.4). Cells remained viable after polyplex delivery, as evaluated with an MTS assay to measure cellular metabolic activity (Figure 3.5). When normalized to cellular metabolic activity, BMP-2 expression was found to increase linearly with increasing E_{gel} for all three cell types, and the linear dependency of BMP-2 expression on E_{gel} was largest for fibroblasts, as compared with BMSCs and myoblasts (Figure 3.6). Untreated cells expressed no BMP-2, and all transfected cells expressed significant levels of BMP-2 relative to untreated controls.

In parallel, cells were transfected with pDNA encoding BMP-2 via electroporation prior to culture on hydrogels with varied elastic moduli in order to evaluate the effects of E_{gel} on exogenous gene expression independent from the effects of E_{gel} on cellular uptake of pDNA. BMP-2 expression from electroporated fibroblasts increased with increasing E_{gel} , similar to fibroblasts transfected with polyplexes in situ. BMP-2 expression from electroporated BMSCs and myoblasts, on the other hand, were independent of E_{gel} (Figure 3.7).

3.4.3 *Effect of matrix stiffness on cell proliferation*

The effects of E_{gel} on cell proliferation were evaluated fibroblasts, BMSCs, and myoblasts using an MTS assay. Absorbance values measured on Day 4 were normalized to those measured on Day 1, and normalized absorbance was found to increase with increasing E_{gel} for all three cell types. The normalized absorbance on 10 kPa gels was significantly lower than that on 320 and 670 kPa gels for all three cell types (Figure 3.8).

3.4.4 *Effect of matrix stiffness on cellular morphology*

The effects of E_{gel} on projected cell area and nuclear aspect ratio were evaluated for fibroblasts (Figure 3.9a-c), BMSCs (Figure 3.9d-f), and myoblasts (Figure 3.9g-i) to evaluate whether these characteristics were related to exogenous BMP-2 expression. For fibroblasts, the projected area increased with increasing E_{gel} and was 1.5 times greater on an E_{gel} of 670 kPa compared to an E_{gel} of 10 kPa. In contrast, the projected area for BMSCs and myoblasts were statistically similar on all E_{gel} (Figure 3.10).

In parallel, the nuclear aspect ratios of cells cultured on hydrogels with varied elastic moduli were calculated from the measured lengths of the major and minor axes of the nuclei. A

nuclear aspect ratio equal to 1 indicates a perfectly circular nucleus, and larger nuclear aspect ratios indicate more elongated nuclei. The nuclear aspect ratios for fibroblasts were significantly greater on an E_{gel} of 670 kPa than an E_{gel} of 320 kPa or 10 kPa, which indicates more elongated nuclei on the stiffest hydrogel. In contrast, the nuclear aspect ratios for BMSCs and myoblasts were independent of E_{gel} (Figure 3.11).

3.5 Discussion

This study uses a cell-adherent PEGDA hydrogel to evaluate the effects of substrate stiffness on non-viral gene delivery for fibroblasts, BMSCs, and myoblasts. pDNA encoding BMP-2 was delivered to cells cultured on fibronectin-conjugated PEGDA hydrogels of varying stiffness. When cells were transfected *in situ* via polyplex delivery, the cellular uptake and subsequent BMP-2 expression for fibroblasts were most dependent on substrate stiffness when compared with BMSCs and myoblasts. When cells were transfected prior to culture via electroporation, BMP-2 expression from fibroblasts was dependent on substrate stiffness while BMP-2 expression from BMSCs and myoblasts were independent of substrate stiffness. To understand the relationship between substrate stiffness and non-viral gene delivery, the effects of substrate stiffness on cell proliferation, projected cell area, and nuclear aspect ratio were evaluated for all three cell types. Fibroblasts, BMSCs, and myoblasts all exhibited an increase in cell proliferation with increasing substrate stiffness while only fibroblasts demonstrated an increase in projected cell area and nuclear elongation with increasing substrate stiffness.

The results from this study indicate that the effects of substrate stiffness on pDNA delivery may be related to both the cellular uptake of pDNA as well as intracellular processes which affect gene expression. The extent to which substrate stiffness influenced BMP-2

expression varied among cell types, likely related to differences in cellular sensitivity to mechanical signals from the matrix. With polyplex delivery, fibroblasts exhibited the most pronounced increase in cellular uptake of pDNA with increasing substrate stiffness when compared with BMSCs and myoblasts, resulting in the most significant increase of BMP-2 expression. BMP-2 expression from BMSCs and myoblasts were less dependent on substrate stiffness compared with fibroblasts, likely related to decreased effects of substrate stiffness on cellular uptake of pDNA. Fibroblasts electroporated with pDNA encoding BMP-2 prior to culture on the hydrogel substrates exhibited an increase in BMP-2 expression with increasing substrate stiffness, suggesting that matrix stiffness may also influence intracellular processes for BMP-2 production since electroporation should normalize any effects of substrate stiffness on cellular uptake of pDNA. In contrast, BMP-2 expression from BMSCs and myoblasts electroporated with pDNA were not dependent on substrate stiffness, implying that effects of substrate stiffness on non-viral gene delivery for BMSCs and myoblasts were related mostly to cellular uptake of pDNA.

Previous studies have indicated that the influence of matrix stiffness on non-viral gene delivery may be primarily due to increased frequency of cell cycle on substrates of increasing stiffness allowing cells to uptake more pDNA (Kong et al, 2005). In this study, however, the effects of substrate stiffness on cellular uptake of pDNA could not be explained solely with changes in cell proliferation. The increase in proliferation of fibroblasts and BMSCs on substrates of increasing stiffness corresponded with increased cellular uptake of pDNA, but to varied extents. Myoblasts, on the other hand, exhibited no significant increase in cellular uptake of pDNA with increasing substrate stiffness despite an increase in proliferation. Results from

this study suggest that the effects of cellular proliferation rate on cellular uptake of pDNA may not be universal for all cell types.

We suggest that substrate stiffness modulates cellular uptake of pDNA by affecting the extent of cell spreading in addition to cellular proliferation rate. The extent of cell spreading has been reported to influence endocytic activities (Adler and Leong, 2010); thus, we suggest that the increased projected area of fibroblasts on stiffer substrates increased endocytosis, resulting in an increased uptake of pDNA. The limited effects of substrate stiffness on the projected cell area of BMSCs and myoblasts, on the other hand, limited the effects of substrate stiffness on cellular uptake of pDNA. In addition, we propose that intracellular processes for gene expression are related to changes in nuclear morphology, as increasing substrate stiffness resulted in significant nuclear elongation for fibroblasts but had minimal effects on nuclear shape for BMSCs and myoblasts. Previous studies have reported that nuclear shape can modulate endogenous gene expression and protein production, possibly due to changes in chromatin structure, though the exact mechanism is unclear (Thomas et al, 2002; Dahl et al, 2008). Similarly, nuclear morphology may be related to exogenous gene expression for fibroblasts in this study, but systematic future studies are needed for better understanding.

This study examined three different cell lines, and it is necessary to examine the role of matrix stiffness on primary cells in future studies. Future work is also needed to extend this study to three-dimensional microenvironments, which more closely mimic conditions found *in vivo*. Previous studies have indicated that gene delivery to cells cultured in three-dimensions is dependent on the pore size within hydrogel matrices (Shepard et al, 2010) as well as matrix stiffness (Gojgini et al, 2011).

Overall, we propose that the results from this study provide important guidelines for developing and improving gene delivery strategies. Therapeutic genes enter a complex microenvironment when administered to the body, and ECM properties, such as stiffness, are known to change with tissue type as well as the age and health conditions of patients (Kong and Mooney, 2007). It is thus valuable to establish a better understanding of the effects of matrix properties on gene delivery. Furthermore, the results from this study will be useful for designing implantable provisional matrices for various gene-based therapies, including tissue regeneration (Shea et al, 1999; Bonadio et al, 1999; Geiger et al, 2005; Huang et al, 2005; Dang and Leong, 2006).

3.6 Conclusion

In conclusion, this study demonstrates that the stiffness of a cell-adherent matrix plays an important role in non-viral gene delivery and that the effects of matrix stiffness are mediated by cell type. Exogenous gene expression from fibroblasts, when compared with that from BMSCs and myoblasts, exhibited the greatest dependency on substrate stiffness. The more pronounced influence of matrix stiffness on non-viral gene delivery for fibroblasts was attributed to a higher sensitivity to changes in matrix stiffness for fibroblasts, as demonstrated by more significant changes in cell area and nuclear aspect ratio, when compared with BMSCs and myoblasts. Ultimately, the results of this study are useful for developing advanced gene delivery strategies and assembling provisional matrices for gene-based therapies.

3.7 References

1. Adler AF and Leong KW. Emerging links between surface nanotechnology and endocytosis: impact on nonviral gene delivery. *Nano Today* 5, 553, 2010.
2. Bonadio J, Smiley E, Patil P, Goldstein S. Localized, direct plasmid gene delivery in vivo: prolonged therapy results in reproducible tissue regeneration. *Nature Medicine* 5, 753, 1999.
3. Dahl KN, Ribeiro AJS, Lammerding J. Nuclear shape, mechanics, and mechanotransduction. *Circulation Research* 102, 1307, 2008.
4. Dang JM and Leong, KW. Natural polymers for gene delivery and tissue engineering. *Advanced Drug Delivery Reviews* 58, 487, 2006.
5. De Laporte L and Shea LD. *Advanced Drug Delivery Reviews* 59, 292, 2007.
6. Dhaliwal A, Lam J, Maldonado M, Lin C, Segura T. Extracellular matrix modulates non-viral gene transfer to mouse mesenchymal stem cells. *Soft Matter* 8, 1451, 2012.
7. Discher DE, Janmey P, Wang YL. Tissue cells feel and respond to the stiffness of their substrate. *Science* 310, 1139, 2005.
8. Engler AJ, Sen S, Sweeney HL, Discher DE. Matrix elasticity directs stem cell lineage specification. *Cell* 126, 677, 2006.
9. Geiger F, Bertram H, Berger I, Lorenz H, Wall O, Eckhardt C, Simank HG, Richter W. Vascular endothelial growth factor gene-activated matrix (VEGF(165)-GAM) enhances osteogenesis and angiogenesis in large segmental bone defects. *Journal of Bone Mineral Res* 20, 2028, 2005.
10. Georges PC and Janmey PA. Cell type-specific response to growth on soft materials. *Journal of Applied Physiology* 98, 1547, 2005.
11. Glover DJ, Lipps HJ, Jans DA. Towards safe, non-viral therapeutic gene expression in humans. *Nature Reviews Genetics* 6, 299, 2005.
12. Gojgini S, Tokatlian T, Segura T. Utilizing cell-matrix interactions to modulate gene transfer to stem cells inside hyaluronic acid hydrogels. *Molecular Pharmaceutics* 8, 1582, 2011.
13. Hsiong SX, Carampin P, Kong HJ, Lee KY, Mooney DJ. Differentiation stage alters matrix control of stem cells. *Journal of Biomedical Materials Research A* 85A, 145, 2008.
14. Huang YC, Simmons C, Kaigler D, Rice KG, Mooney DJ. Bone regeneration in a rat cranial defect with delivery of PEI-condensed plasmid DNA encoding for bone morphogenetic protein-4 (BMP-4). *Gene Therapy* 12, 418, 2005.

15. Khatiwala CB, Peyton SR, Putnam AJ. Intrinsic mechanical properties of the extracellular matrix affect the behavior of pre-osteoblastic MC3T3-E1 cells. *American Journal of Physiology – Cell Physiol* 290, C1640, 2006.
16. Kirker-Head CA. Potential applications and delivery strategies for bone morphogenetic proteins. *Advanced Drug Delivery Reviews* 43, 65, 2000.
17. Kong HJ, Hsiong S, Mooney DJ. Nanoscale cell adhesion ligand presentation regulates nonviral gene delivery and expression. *Nano Letters* 7, 161, 2007.
18. Kong HJ, Liu JD, Riddle K, Matsumoto T, Leach K, Mooney DJ. Non-viral gene delivery regulated by stiffness of cell adhesion substrates. *Nature Materials* 4, 460, 2005.
19. Kong HJ and Mooney DJ. Microenvironmental regulation of biomacromolecular therapies. *Nature Reviews Drug Discovery* 6, 455, 2007.
20. Lieberman JR, Daluiski A, Stevenson S, Wu L, McAllister P, Lee YP, Kabo JM, Finerman GAM, Berk AJ, Witte ON. The effect of regional gene therapy with bone morphogenetic protein-2-producing bone-marrow cells on the repair of segmental femoral defects in rats. *Journal of Bone and Joint Surgery* 81A, 905, 1999.
21. Luo D and Saltzman WM. Synthetic DNA delivery systems. *Nature Biotechnology* 18, 33, 2000.
22. Mintzer MA and Simanek EE. Nonviral Vectors for Gene Delivery. *Chemical Reviews* 109, 259, 2009.
23. O'Rourke S, Keeney M, Pandit A. Non-viral polyplexes: Scaffold mediated delivery for gene therapy. *Progress in Polymer Science* 35, 441, 2010.
24. Pack DW, Hoffman AS, Pun S, Stayton PS. Design and development of polymers for gene delivery. *Nature Reviews Drug Discovery* 4, 581, 2005.
25. Pouton CW and Seymour LW. Key issues in non-viral gene delivery. *Advanced Drug Delivery Reviews* 46, 187, 2001.
26. Putnam D. Polymers for gene delivery across length scales. *Nature Materials* 5, 439, 2006.
27. Rose LC, Kucharski C, Uludag H. Protein expression following non-viral delivery of plasmid DNA coding for basic FGF and BMP-2 in a rat ectopic model. *Biomaterials* 33, 3363, 2012.
28. Shea LD, Smiley E, Bonadio J, Mooney DJ. DNA delivery from polymer matrices for tissue engineering. *Nature Biotechnology* 17, 551, 1999.

29. Shepard JA, Huang A, Shikanov A, Shea LD. Balancing cell migration with matrix degradation enhances gene delivery to cells cultured three-dimensionally within hydrogels. *Journal of Controlled Release* 146, 128, 2010.
30. Storrie H and Mooney DJ. Sustained delivery of plasmid DNA from polymeric scaffolds for tissue engineering. *Advanced Drug Delivery Reviews* 58, 500, 2006.
31. Thomas CH, Collier JH, Sfeir CS, Healy KE. Engineering gene expression and protein synthesis by modulation of nuclear shape. *Proceedings of the National Academy of Sciences USA* 99, 1972, 2002.
32. Wiethoff CM and Middaugh CR. Barriers to nonviral gene delivery. *Journal of Pharmaceutical Science* 92, 203, 2003.
33. Yeung T, Georges PC, Flanagan LA, Marg B, Ortiz M, Funaki M, Zahir N, Ming WY, Weaver V, Janmey PA. Effects of substrate stiffness on cell morphology, cytoskeletal structure, and adhesion. *Cell Motility and the Cytoskeleton* 60, 24, 2005.

3.8 Figures

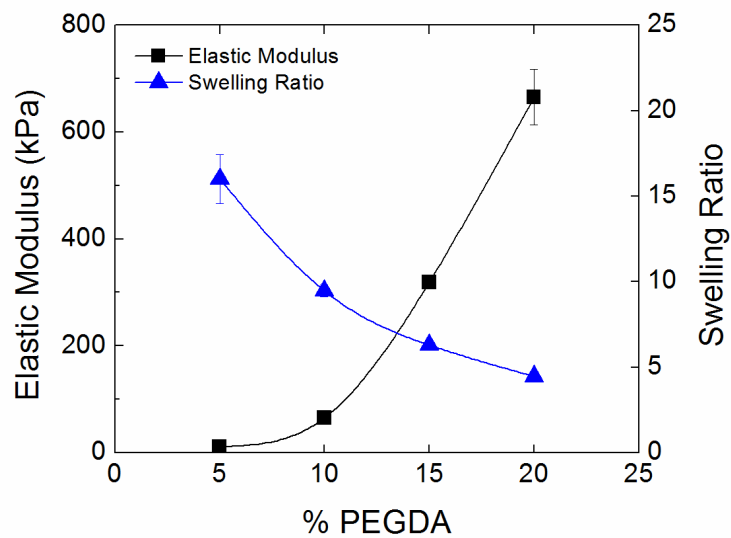


Figure 3.1 PEGDA Hydrogel characterization. Elastic moduli (■) and swelling ratios (▲) of PEGDA hydrogels controlled by PEGDA concentration. As the PEGDA concentration was increased from 5 to 20%, the elastic modulus increased from 10 to 670 kPa while the swelling ratio decreased from 16 to 4.5.

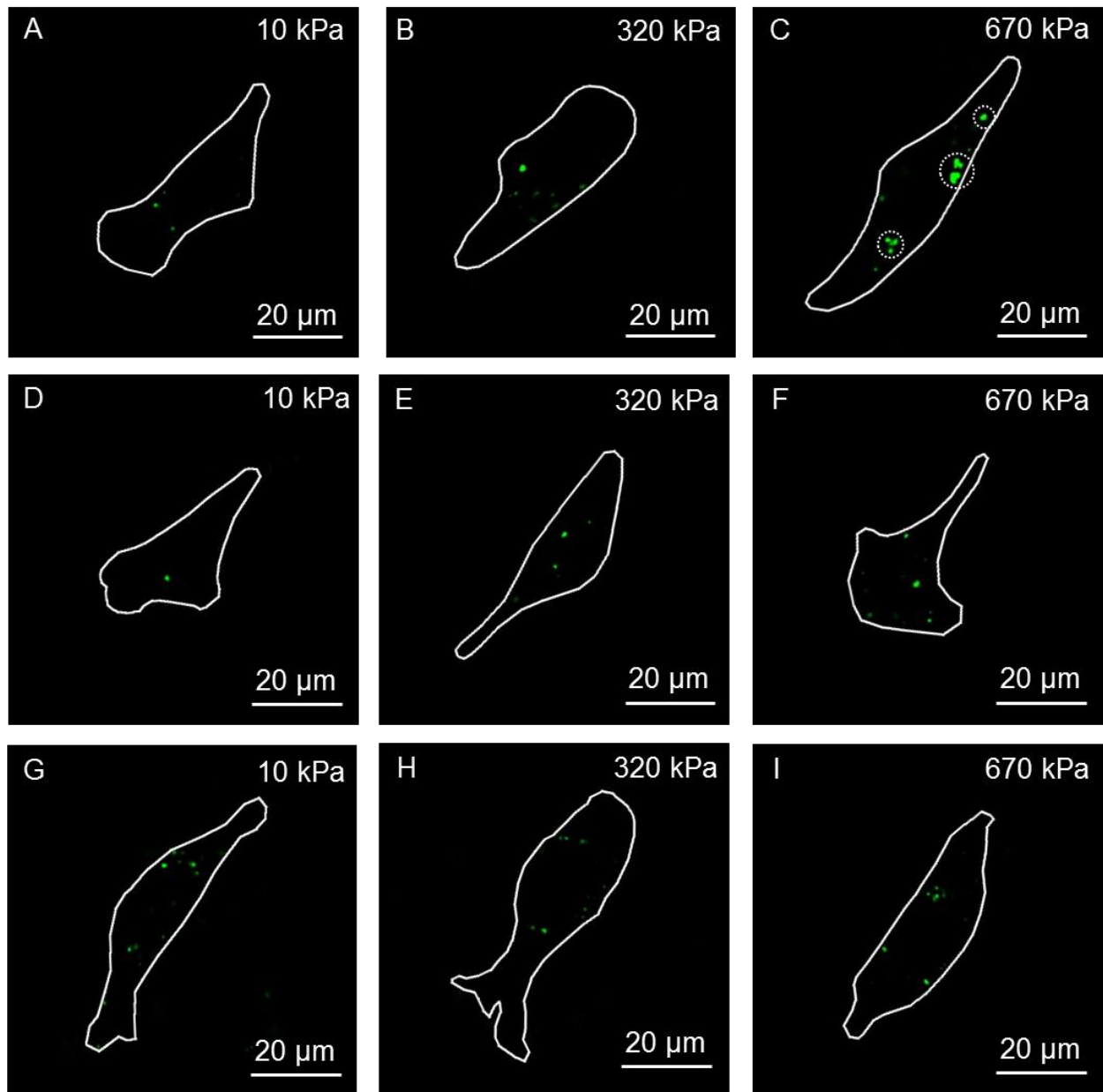


Figure 3.2 Uptake of fluorescently-labeled pDNA. Fluorescent images of cellular uptake of pDNA for NIH3T3 fibroblasts (a-c), D1 BMSCs (d-f), and C2C12 myoblasts (g-i) cultured on 10, 320, and 670 kPa hydrogels.

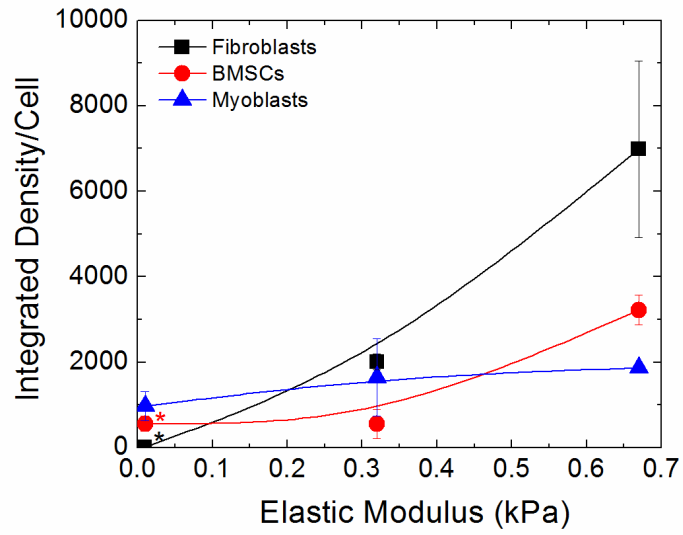


Figure 3.3 Quantification of cellular uptake of pDNA. The cellular uptake of fluorescently-labeled pDNA to fibroblasts (■), BMSCs (●), and myoblasts (▲) as evaluated with integrated density from fluorescent images. Cellular uptake of pDNA on 10 kPa gels was statistically different from that on 320 and 670 kPa gels for fibroblasts and BMSCs (* $p < 0.05$). Values and error bars represent the mean and standard deviation characterized from four independent images, each containing at least ten cells.

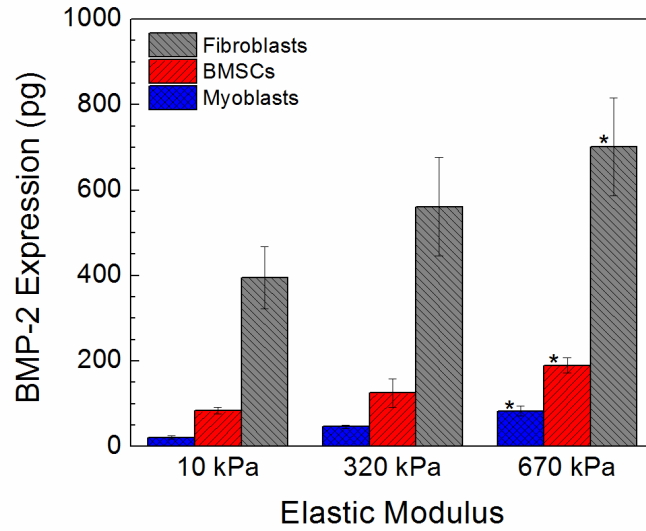


Figure 3.4 Effects of substrate stiffness on absolute BMP-2 expression. BMP-2 expression in picograms resulting from in situ delivery of polyplexes containing pDNA encoding BMP-2 to NIH3T3 fibroblasts, D1 BMSCs, and C2C12 myoblasts cultured on fibronectin-conjugated PEGDA hydrogels with elastic moduli of 10, 320, and 670 kPa. Differences between BMP-2 expression levels on the stiffest (670 kPa) and softest (10 kPa) gels were statistically significant for all cell types (* $p < 0.05$). Values and error bars represent the mean and standard deviation characterized from four independent samples.

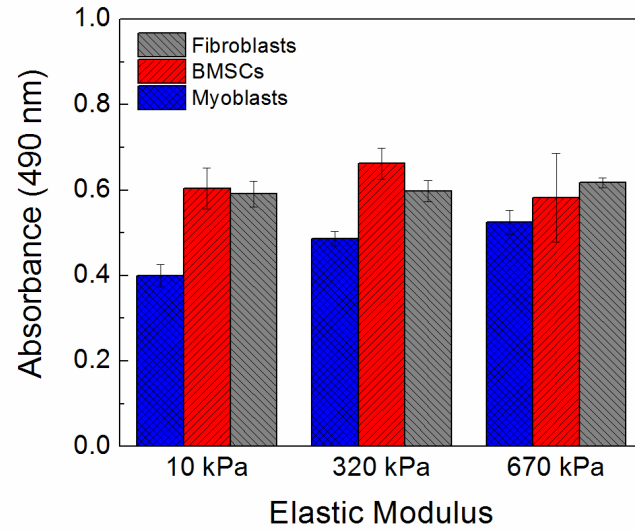


Figure 3.5 Effects of substrate stiffness on cellular metabolic activity. Cellular metabolic activity, as evaluated with an MTS assay, for NIH3T3 fibroblasts, D1 BMSCs, and C2C12 myoblasts cultured on fibronectin-conjugated PEGDA hydrogels with elastic moduli of 10, 320, and 670 kPa. Values and error bars represent the mean and standard deviation characterized from four independent samples.

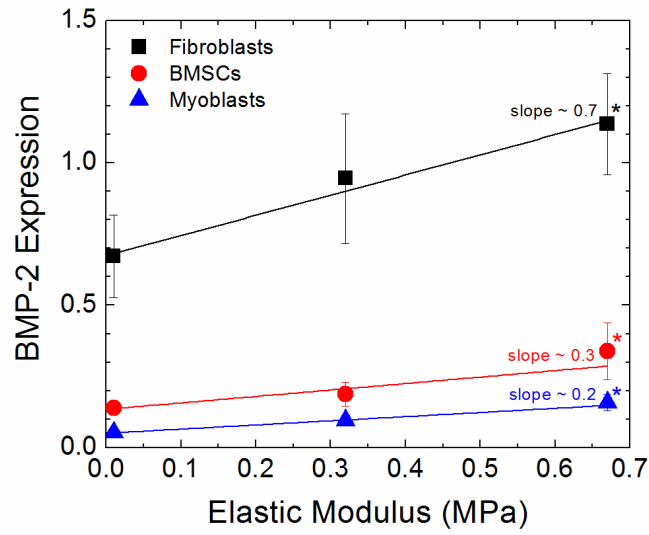


Figure 3.6 Effects of substrate stiffness on normalized BMP-2 expression. BMP-2 expression, measured in nanograms, was normalized to cellular metabolic activity, as evaluated with absorbance from an MTS assay for fibroblasts (■), BMSCs (●), and myoblasts (▲). Differences between normalized BMP-2 expression on the stiffest (670 kPa) and softest (10 kPa) gels were statistically significant for all cell types (* $p < 0.05$). Values and error bars represent the mean and standard deviation characterized from four independent samples from each experiment.

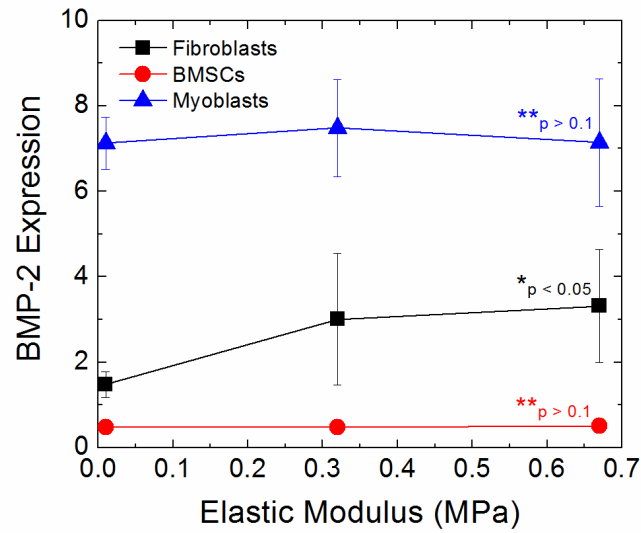


Figure 3.7 Effects of substrate stiffness on BMP-2 expression from electroporation. BMP-2 expression from NIH3T3 fibroblasts (■), D1 BMSCs (●), and C2C12 myoblasts (▲) electroporated with pDNA encoding BMP-2 prior to culture on fibronectin-conjugated PEGDA hydrogels with elastic moduli of 10, 320, and 670 kPa. BMP-2 expression, measured in nanograms, was normalized to cellular metabolic activity, as evaluated with absorbance from an MTS assay. Differences between BMP-2 expression on the stiffest (670 kPa) and softest (10 kPa) gels were statistically significant for fibroblasts (* $p < 0.05$). BMP-2 expression on the stiffest (670 kPa) and softest (10 kPa) gels were statistically similar for BMSCs and myoblasts (** $p > 0.1$). Values and error bars represent the mean and standard deviation characterized with from four independent samples.

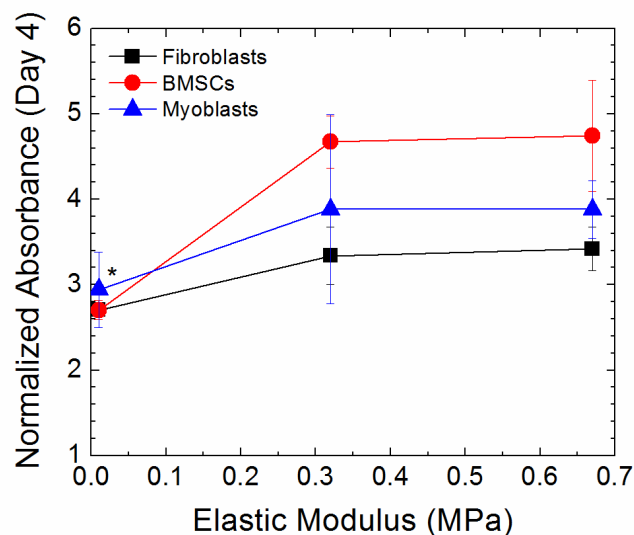


Figure 3.8 Effects of substrate stiffness on cell proliferation. Proliferation of NIH3T3 fibroblasts (■), D1 BMSCs (●), and C2C12 myoblasts (▲), as evaluated with normalized absorbance values from an MTS assay after four days of culture on fibronectin-conjugated PEGDA hydrogels with elastic moduli of 10, 320, and 670 kPa. For each cell type and elastic modulus, absorbance values measured on Day 4 were normalized to those measured on Day 1. Normalized absorbance on 10 kPa gels were statistically different from that on 320 and 670 kPa gels for all three cell types (* $p < 0.05$). Values and error bars represent the mean and standard deviation characterized from four independent samples.

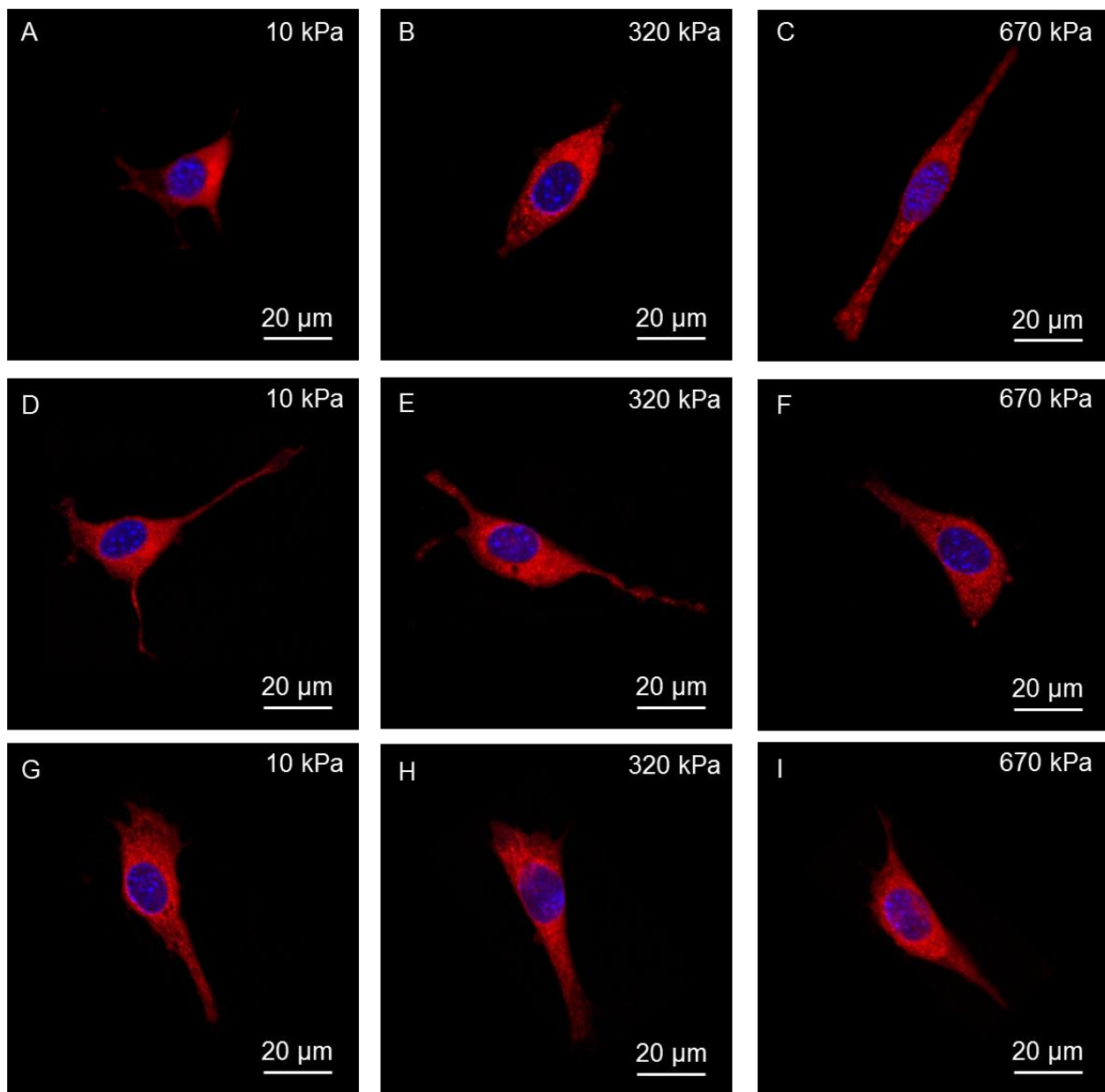


Figure 3.9 Analysis of cellular morphology. Fluorescent images of NIH3T3 fibroblasts (a-c), D1 BMSCs (d-f), and C2C12 myoblasts (g-i) cultured on fibronectin-conjugated PEGDA hydrogels with elastic moduli of 10, 320, and 670 kPa. The cell membranes (red) and nuclei (blue) were stained with a CellMask Deep Red Plasma Membrane Stain and DAPI, respectively.

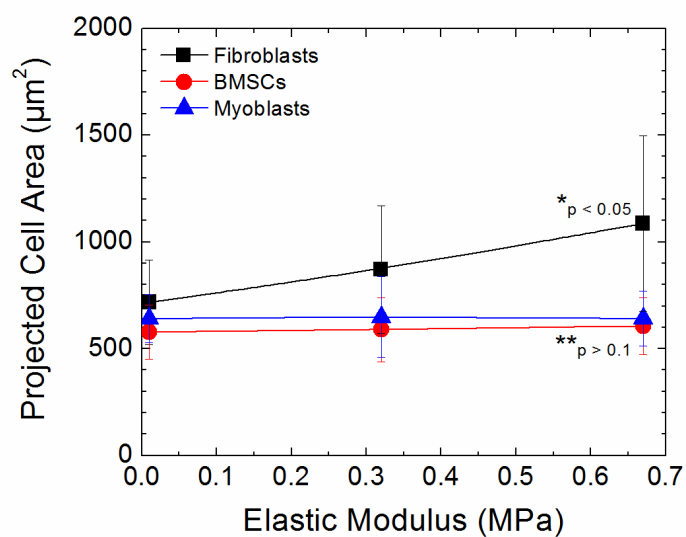


Figure 3.10 Effects of substrate stiffness on projected cell area. Projected cell area for NIH3T3 fibroblasts (■), D1 BMSCs (●), and myoblasts (▲) cultured on fibronectin-conjugated PEGDA hydrogels with elastic moduli of 10, 320, and 670 kPa. Differences between projected cell area on the stiffest (670 kPa) and softest gels (10 kPa) were statistically significant for fibroblasts (* $p < 0.05$). Projected cell area on the stiffest (670 kPa) and softest (10 kPa) gels were statistically similar for BMSCs and myoblasts (** $p > 0.1$). Values and error bars represent the mean and standard deviation characterized from twenty independent, randomly-selected cells.

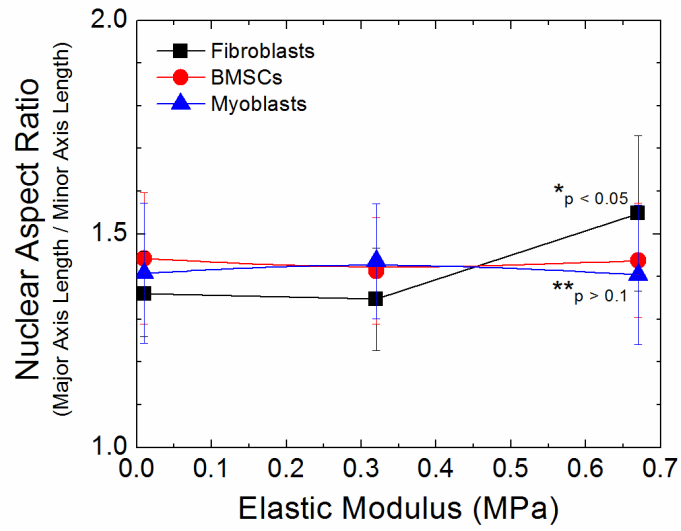


Figure 3.11 Effects of substrate stiffness on nuclear aspect ratio. Nuclear aspect ratio for NIH3T3 fibroblasts (■), D1 BMSCs (●), and C2C12 myoblasts (▲) cultured on fibronectin-conjugated PEGDA hydrogels with elastic moduli of 10, 320, and 670 kPa. Differences between nuclear aspect ratios on the stiffest (670 kPa) and softest (10 kPa) gels were statistically significant for fibroblasts (* $p < 0.05$). Nuclear aspect ratios on the stiffest (670 kPa) and softest (10 kPa) gels were statistically similar for BMSCs and myoblasts (** $p > 0.1$). Values and error bars represent the mean and standard deviation characterized from twenty independent, randomly-selected cells.

CHAPTER 4: MICROVASCULAR STAMP WITH GENETICALLY MODIFIED CELLS FOR REVASCULARIZATION THERAPIES

4.1 Introduction

Revascularization therapies have the potential to treat a wide array of diseases, including ischemic disease and cardiovascular disease, which is the leading cause of death in the United States (Lei et al, 2005; Heron et al, 2009). Revascularization is also critical for wound healing and tissue regeneration. Tissues thicker than 100 μm must be vascularized for the transport of oxygen and nutrients due to diffusion limitations (Khademhoseini et al, 2009). This has thus far been a limiting factor in repairing and regenerating thick or complex tissues (Levenberg et al, 2005; Rouwkema et al, 2008). In efforts to restore blood flow to ischemic tissues or to vascularize engineered tissues, angiogenic proteins or genes can be administered to stimulate angiogenesis, which refers to the formation of new blood vessels from existing vasculature (Lei et al, 2004).

Vascular endothelial growth factor (VEGF) has been widely investigated for use in revascularization therapies and has been shown to support angiogenesis both *in vitro* and *in vivo* (Ferrara et al, 2003). Specifically, delivery of non-viral genes encoding VEGF has been increasingly studied to stimulate angiogenic activities in a more sustained manner than direct protein delivery. In order to further improve the efficacy of genes encoding VEGF, plasmid DNA encoding VEGF are frequently encapsulated in biomaterial scaffolds for implantation (Zisch et al, 2003; Kong et al, 2008). Alternatively, cells genetically manipulated to express VEGF *ex vivo* can be transplanted to stimulate angiogenesis, and such use of genetically modified cells may be advantageous in facilitating localized expression for angiogenic therapies. However, this approach is still limited by difficulties in regulating the level of cellular exogenous

expression of VEGF (Lei et al, 2004). The dose of VEGF is critical for therapeutic applications, as high doses of VEGF result in abnormal angiogenesis (Ozawa et al, 2004; Ehrbar, 2004).

For successful revascularization therapies, it is critical to control the number, size, spacing, and maturity of neovessels at the target site (Dor et al, 2003; Chen et al, 2007); however, technologies to do so are still lacking. Previous studies have demonstrated that blood vessel formation can be regulated by controlling the spatio-temporal delivery of angiogenic factors (Silva et al, 2010). For example, a bilayer scaffold synthesized to control the temporal delivery of VEGF was shown to regulate the density, size, and maturity of newly formed blood vessels (Chen et al, 2007). While such studies provide crucial insight to regulating the formation of new blood vessels, precise patterning of functional blood vessels at physiologically relevant length-scales remains a challenge. Various microfabrication techniques have been used to pattern molecules or cells for tissue engineering applications and biological studies (Khademhosseini et al, 2006), but such techniques are still unable to direct blood vessel formation.

Recently, researchers in the Kong Lab developed a “living” microvascular stamp that was able to release multiple angiogenic factors to support neovessel formation along microchannels in the stamp. The stamp incorporated cells that secrete angiogenic factors in a three-dimensional hydrogel matrix to promote cellular expression of angiogenic factors. Upon implantation in an *in vivo* angiogenesis model, the stamp promoted the desired pattern of neovessels based on its 3D geometry and allowed for controlled spacing and density of neovessel formation (Jeong et al, 2011; Figure 4.1). It is proposed that the efficacy of this vascular stamp be further improved with a more refined control of angiogenic growth factor expression from the encapsulated cells. Therefore, it would be valuable to incorporate cells transfected with plasmid DNA (pDNA)

encoding VEGF into the microvascular stamp to potentially control VEGF expression with pDNA dose, cell density, and matrix properties.

4.2 Objective and scope

We hypothesize that the microvascular stamp containing cells transfected with pDNA encoding VEGF will release VEGF along pre-defined microchannel patterns and promote formation of micro-sized blood vessels according to the microchannels engraved into the stamp. Furthermore, the viability of transfected cells and exogenous production of VEGF in the stamp will be tuned with the dosage of pDNA encoding VEGF and permeability of the hydrogel. To examine this hypothesis, NIH3T3 fibroblasts were first transfected with varying amounts of pDNA encoding VEGF₁₆₅ to evaluate cell viability and VEGF production. Then, the cells transfected with the proper dose of pDNA were used to assemble a microvascular stamp (Jeong et al, 2011). These cells were encapsulated in a hydrogel system consisting of poly(ethylene glycol) diacrylate (PEGDA) of different molecular weights or a mixture of PEGDA and methacrylic alginate (MA) using a stereolithography apparatus (SLA). The hydrogel permeability and subsequent cell viability were controlled with the molecular weight of PEGDA and the addition of MA. The SLA unit was used to fabricate microchannels within the hydrogel structure to direct blood vessel growth. The resulting microvascular stamp was implanted on a chick chorioallantoic membrane (CAM) to assess neovessel formation *in vivo*.

4.3 Materials and methods

4.3.1 *Methacrylic alginate synthesis*

The alginate used in this study (molecular weight $\sim 50,000$ g/mol) was obtained by irradiating alginate rich in gluronic acid residues (LF20/40, FMC Biopolymer, Philadelphia, PA) with a cobalt-60 source for 4 hours at a dose of 5.0 Mrad (Kong et al, 2002). 2-aminoethylmethacrylate (Sigma Aldrich, St. Louis, MO) was conjugated to alginate using carbodiimide chemistry (Figure 4.2). In brief, alginate was dissolved in 0.1 M 2-(N-morpholino) ethanesulfonic acid (MES, Sigma Aldrich) buffer at a concentration of 1% (w/v). Hydroxybenzotriazole (HOBt, Sigma), 1-ethyl-3-(3-dimethylaminopropyl) carbodiimide (EDC, Thermo Scientific, Rockford, IL), and 2-aminoethylmethacrylate were added to the alginate solution and stirred. The molar ratios of HOBt to 2-aminoethylmethacrylate and EDC to 2-aminoethylmethacrylate were both kept constant at 2:1. After the mixture was allowed to react for 18 hours, the solution was dialyzed extensively against deionized water for three days while changing the deionized water every 12 hours. Finally, the dialyzed solution was lyophilized and reconstituted to a 3 wt % stock solution. For this study, the number of acrylate groups conjugated to each alginate chain was kept constant at 60 as confirmed by $^1\text{H-NMR}$ (300 MHz, QE-300, General Electric), as previously reported (Cha et al, 2009).

4.3.2 *Poly(ethylene glycol) diacrylate synthesis*

Poly(ethylene glycol) diacrylate (PEGDA) was synthesized from poly(ethylene glycol) (PEG, molecular weight ~ 1000 g/mol, Sigma Aldrich) and acryloyl chloride (Sigma Aldrich). PEG was first dissolved in dichloromethane at a concentration of 10 wt %. Acryloyl chloride and triethylamine (Fisher Chemical, Fairlawn, NJ) were added to the PEG solution and stirred

under dry N₂ gas (Figure 4.3). PEG, acryloyl chloride, and triethylamine were added at a ratio of 1:4:4. After the mixture was allowed to react overnight, the insoluble triethylamine-HCl byproduct was removed by filtration. The PEGDA₁₀₀₀ product in the remaining solution was then precipitated by adding ice-cold ether. The precipitated crude product was dissolved in deionized water and dialyzed for one day to remove any byproducts or unreacted starting materials and lyophilized. The conjugation of acrylate groups on PEG was confirmed by ¹H-NMR (300 MHz, QE-300, General Electric).

4.3.3 *Hydrogel formulation and analysis*

Hydrogels were prepared from methacrylic alginate, PEGDA₁₀₀₀ (molecular weight of repeat unit ~ 1000 g/mol), and PEGDA₄₀₀ (molecular weight of repeat unit ~ 400 g/mol, Polysciences, Inc., Warrington, PA) through photopolymerization. PEGDA₄₀₀, PEGDA₁₀₀₀, and PEGDA₁₀₀₀-MA solutions were prepared in Dulbecco's modified Eagle's medium (DMEM; Invitrogen, Carlsbad, CA) at constant solids concentrations of 10% w/v. PEGDA₄₀₀ and PEGDA₁₀₀₀ solutions contained 10% w/v PEGDA in DMEM. PEGDA₁₀₀₀-MA solutions contained 8.5% w/v PEGDA and 1.5% w/v MA in DMEM. A 10% w/v solution of the photoinitiator, Irgacure 2959 (Ciba, Tarryton, NY), was prepared in dimethyl sulfoxide (DMSO, Fisher Chemical), and 10 µl of the resulting stock solution was added to 1 ml of the pregel solution. The mixture was then poured between glass plates with a 1mm spacer and exposed to ultraviolet light using a CHiPhERASER Model 20 (Jelight Company Inc, Irvine, CA) for 10 minutes. Hydrogel disks were punched using a 5 mm puncher and incubated in phosphate buffered saline (PBS, Invitrogen).

The swelling ratio of the hydrogels was quantified with the mass ratio of hydrated disks

to dried disks. The average pore size (ζ) within PEGDA cross-linked networks was calculated from Eq 1 (Raeber et al, 2005):

$$\zeta = (\nu_{2,s}^{-1/3})(\bar{r}_0^2)^{1/2} \quad \text{Eq 1}$$

where $\nu_{2,s}$ represents the polymer volume fraction gel in the swollen state, which is equal to the inverse of the swelling ratio, and $(\bar{r}_0^2)^{1/2}$ represents the unperturbed mean-square end-to-end distance of the molecule. For alginate, this value is 254 nm. For PEG, $(\bar{r}_0^2)^{1/2}$ was calculated from Eq 2:

$$(\bar{r}_0^2)^{1/2} = nlC_n \quad \text{Eq 2}$$

Where n represents the number of repeat units, l represents the average monomer length (1.46 Å), and C_n represent the characteristic ratio for PEG (= 4).

4.3.4 Cell culture and transfection

NIH3T3 fibroblasts (ATCC, Manassas, VA) were cultured in DMEM supplemented with 10% fetal bovine serum (FBS; Invitrogen) and 100 units/mL penicillin-streptomycin (Invitrogen) at 37°C in a 5% CO₂ incubator. Plasmid DNA (pDNA) encoding VEGF₁₆₅ was first obtained from Dr. Douglas Losordo (Northwestern University) and expanded by Aldevron (Fargo, ND). Cells were transfected with plasmid pDNA encoding VEGF₁₆₅ through electroporation with the Neon Transfection System (Invitrogen). With the Neon Transfection System 100 µl Kit, cells were suspended in Buffer R at a density of 50×10^6 cells/ml. pDNA was added to the cell suspension at varying concentrations, and 100 µl of the resulting solution was aspirated into each Neon Transfection Tip. Cells were electroporated with 2 pulses of 1350 V for 20 ms after which the contents of the tip were ejected into complete growth media without antibiotics. For cell

encapsulation experiments, cells were electroporated in a solution that contained 0.1 $\mu\text{g}/\mu\text{l}$ pDNA and cultured for 24 hours prior to encapsulation.

4.3.5 Cell encapsulation in hydrogels

Cells were encapsulated in 1 mm thick hydrogels prepared using a CHiPhERASER Model 20 as described above. For encapsulation within this hydrogel system, cells were mixed with PEGDA₄₀₀, PEGDA₁₀₀₀, and PEGDA₁₀₀₀-MA pregel solutions at a cell density of 1 million cells/ml. The solutions were polymerized as described above. Disks were punched and placed directly into complete growth media for culture in a 37°C, 5% CO₂ incubator. Cell viability was analyzed 4 hours and 24 hours after encapsulation with MTS tetrazolium [3-(4,5-dimethylthiazol-2-yl)-5-(3-carboxymethoxyphenyl)-2-(4-sulfophenyl)-2H-tetrazolium, inner salt] (Promega Corporation, Madison, WI). In brief, cell viability was indicated by the formation of a soluble formazan product after treatment with the MTS reagent. The amount of formazan produced was quantified with absorbance at 490nm, and the quantity of formazan measured was directly proportional to the number of viable cells in culture.

4.3.6 Cell encapsulation in microvascular stamps using SLA

Cells were mixed with the pre-gel solution at a density of 5 million cells/ml or 10⁵ cells/ml. The pre-gel solution consisted of 18.5 % w/v PEGDA and 1.5% w/v MA dissolved in DMEM. The photoinitiator, Irgacure 2959, was added to the pre-gel solution at a final concentration of 0.2% w/v. A stereolithography apparatus (SLA, Model 250/50, 3D Systems, Rock Hill, South Carolina) was used to photopolymerize the pre-gel solution to form hydrogels

(Figure 4.4). The resulting hydrogels were cylindrical disks with diameters of 5 mm and thicknesses of 200 μm , as specified with a computer-aided design (CAD) model.

4.3.7 *Cell viability and VEGF secretion assays*

For *in vitro* experiments to evaluate the optimal pDNA concentration for electroporation, cells were electroporated with varying pDNA concentrations, and 5,000 cells were plated in 100 μl complete growth media without antibiotics. The media was changed every 24 hours and collected on Days 1, 2, and 4 for VEGF analysis. Cell viability was analyzed in parallel with an MTS reagent, as described above. For *in vitro* experiments to evaluate VEGF secretion from microvascular stamps, the media was collected four hours after fabrication and on Days 1, 4, and 7 for VEGF analysis. Cell viability was analyzed in parallel with an MTS reagent.

The amount of VEGF present in the media collected from *in vitro* studies was quantified with a VEGF enzyme-linked immunosorbant assay (ELISA, R&D Systems, Minneapolis, MN). In brief, microplates were coated with mouse anti-human VEGF₁₆₅. The samples to be assayed were then incubated on the microplate and allowed to bind to the immobilized antibodies. Next, biotinylated mouse anti-human VEGF₁₆₅ was added, followed by streptavidin conjugated to horseradish-peroxidase. Finally, upon addition of a substrate solution, the absorbance of the final solution at 450 nm and 540 nm were measured with a Synergy HT plate reader (BioTek, Winooski, VT). The absorbance at 540 nm was subtracted from the absorbance at 450 nm, and the amount of VEGF detected was calculated from a calibration curve established using VEGF standards.

4.3.8 Chorioallontic membrane-based angiogenesis assay

Embryonic chicken eggs (Hy-Line W-36, Poultry Research Farm, University of Illinois, Urbana, Illinois) were incubated at 37°C with 5% CO₂. On the ninth day of gestation, a small window (1 cm × 1cm) was created in each egg shell. After an additional day of incubation to stabilize the embryos, hydrogel disks were implanted on each chorioallontic membrane (CAM) (Figure 4.5). After 7 days of incubation with the hydrogel disks, the membranes were fixed with 10% neutral buffered formalin (NBF) for 20 hours for further analysis. CAM images were captured using a Leica S6C stereomicroscope.

4.4 Results and discussion

4.4.1 Effects of pDNA dosage on gene expression and cell viability

NIH3T3 fibroblasts were electroporated with varying doses of plasmid DNA (pDNA) encoding vascular endothelial growth factor (VEGF). The concentration of pDNA in the electroporation medium was varied from 0 µg/µl to 0.3 µg/µl, and the resulting cell viability and VEGF secretion were evaluated on Days 1, 2, and 4 after initially plating 5,000 cells. With a pDNA dose of 0 µg/µl, cells did not express any detectable VEGF (data not shown). As the concentration of pDNA was increased from 0.05 to 0.2 µg/µl, the VEGF expression increased from 2 to 46 ng after 1 day. Further increase of pDNA dosage to 0.3 µg/µl resulted in no statistically significant increase in VEGF expression (Figure 4.6). The cellular VEGF production decreased significantly on Day 4, regardless of the pDNA dosage.

Relative cell viability was also evaluated by normalizing the viability of transfected cells to the viability of cells electroporated with 0 µg/µl pDNA. Increasing the pDNA dosage from 0.05 to 0.1 µg/µl, which increased VEGF expression from 1 to 40 ng on Day 2, had minimal

effects on cell viability. As the concentration of pDNA was increased further from 0.1 $\mu\text{g}/\mu\text{l}$ to 0.2 $\mu\text{g}/\mu\text{l}$, minimal changes in VEGF expression were observed, and the relative cell viability decreased significantly (Figure 4.7). These results demonstrate that a pDNA dosage between 0.05 and 0.1 $\mu\text{g}/\mu\text{l}$ would be appropriate to stimulate cellular exogenous production of VEGF while retaining cell viability.

4.4.2 Effects of polymer composition on hydrogel pore size and viability of encapsulated cells

Hydrogel disks of three different compositions were prepared from a solution containing 10% w/v PEGDA₄₀₀, a solution containing 10% w/v PEGDA₁₀₀₀, and a solution containing 8.5% PEGDA₁₀₀₀ and 1.5% MA. The swelling ratios of the resulting hydrogel disks were quantified and used to calculate the average pore size within the hydrogel network using Eq 1 and Eq 2. For PEGDA hydrogels, increasing the molecular weight from 400 to 1000 increased the average pore size from 11 nm to 30 nm. The addition of MA further increased the swelling ratio of the hydrogels, and the resulting pore size, as calculated from the unperturbed mean-square end-to-end distance of both PEG and alginate, increased to 121 nm (Figure 4.8). The viability of encapsulated cells increased with increasing hydrogel permeability, as characterized with pore size. While cells were not viable in PEGDA₄₀₀ gels, the increased permeability of PEGDA₁₀₀₀ gels were able to support cell viability. Incorporation of MA further increased cell viability, though the difference was not statistically significant within 24 hours of encapsulation (data not shown). We envisage, however, that the difference between conditions will increase with a longer incubation period.

4.4.3 *Cell viability and VEGF secretion from microvascular stamps*

First, NIH3T3 fibroblasts transfected with pDNA encoding VEGF were incorporated in hydrogel microvascular stamps using SLA at a cell density of 5 million cells/ml. Based on studies conducted in Section 4.4.2, the microvascular stamp was prepared by cross-linking PEGDA₁₀₀₀ and MA. Cells remained viable after the fabrication process, as exhibited with an MTT stain 24 hours following encapsulation (Figure 4.9). The amount of VEGF secreted four hours after fabrication and the amount of VEGF secreted on Days 1, 4, and 7 were quantified. The cell viability was analyzed in parallel. Four hours after encapsulation, no detectable VEGF was released from the microvascular stamp (data not shown). After 24 hours, significant amounts of VEGF were released from the vascular stamp. The amount of VEGF released from the vascular stamp decreased over seven days (Figure 4.10), but the 8 ng released on Day 7 is within the concentration needed to stimulate angiogenesis (Jeong et al, 2011). Cell viability was analyzed on Days 1, 4, and 7 and normalized to cell viability 4 hours after fabrication. A majority of the cells in the vascular stamp remained viable up to Day 4, but viability decreased by Day 7 (Figure 4.11). However, it is noteworthy that more than 50% of the cells remained viable in a 3D hydrogel matrix during 7 days of encapsulation, which is difficult to achieve with a conventional synthetic hydrogel system.

Overall, we suggest that the gradual decrease in cellular exogenous VEGF production during the first four days of culture results from intrinsic gene silencing mechanisms, such as cytosine methylation (Hong et al, 2001; Glover et al, 2005), and not early cell death. The continued decrease of VEGF production between Days 4 and 7 may be attributed to both intrinsic gene silencing and cell death. Despite the decrease in VEGF production, these results indicate that the microvascular stamp consisting of a permeable hydrogel with cells modified to

produce VEGF could release angiogenic factors at an implant site, as described in the following section.

4.4.4 Blood vessel formation from microvascular stamps in a CAM-based angiogenesis assay

Finally, the hydrogel-based vascular stamps were implanted on a chorioallantoic membrane (CAM). The vascular stamps were assembled with a permeable PEGDA₁₀₀₀-MA hydrogel and fabricated with 500 μm -diameter microchannels. NIH3T3 fibroblasts transfected with pDNA encoding VEGF were incorporated in the microvascular stamps at a density of 10^5 cells/ml. When implanted on a CAM, this microvascular stamp stimulated the growth of neovessels along its circular patterns (Figure 4.12A). In addition, the patterned neovessels were connected, suggesting that new capillaries sprouted from neighboring blood vessels. In contrast, no patterned neovessels formed when the microvascular stamps were constructed with cells that had not been transfected with pDNA encoding VEGF (Figure 4.12B).

Increasing the density of cells within the microvascular stamps to 5×10^6 cells/ml resulted in a pro-inflammatory response, characterized by the formation of fibrous tissue on the surface of the vascular stamp (Figure 4.13). In contrast, inflammation was not observed on stamps fabricated with cells that had not been transfected with pDNA encoding VEGF at the same cell density (data not shown). This result demonstrates the importance of VEGF dosage, which was controlled by cell density in this study, in stimulating either neovessel formation or pro-inflammation.

We propose that the microvascular stamp combined with a gene delivery strategy in this study is advantageous over the previous microvascular stamp, which was equipped with cells chemically stimulated to express endogenous angiogenic factors. The expression level of

angiogenic factors can be more readily tuned in the microvascular stamp used in this study. It would also be possible to combine these VEGF-producing cells with other cells transfected with pDNA encoding supplemental angiogenic growth factors, such as Angiopoietin or platelet-derived growth factor (PDGF). Furthermore, we envisage that the VEGF expression level in the microvascular stamp could be further tuned with the mechanical and chemical properties of a hydrogel matrix, as discussed in previous chapters, as well as the permeability of the hydrogel matrix. Overall, the microvascular stamp from this study could potentially be used to promote the formation of organized vasculatures and facilitate transport in tissue regeneration therapies or engineered 3D tissues.

4.5 Conclusion

Overall, this study demonstrates that a microvascular stamp equipped with cells genetically manipulated to produce exogenous VEGF is able to control the growth and spacing of blood vessels. The dosage of pDNA encoding VEGF, the hydrogel permeability, and the cell density were all factors in controlling the amount of VEGF released along the microchannels to control neovessel formation while circumventing host inflammation. Specifically, the pDNA dosage and hydrogel permeability were key factors in retaining cell viability in a 3D matrix, and cell density was an important factor in tuning the balance between angiogenesis and inflammation. We propose that this microvascular stamp, which incorporates gene delivery strategies, may be useful in improving the quality of revascularization therapies.

4.6 References

1. Cha C, Kohman RE, Kong H. Independent control of stiffness, toughness, and hydrogel degradation rate. *Advanced Functional Materials* 19, 3056, 2009.
2. Chen RR, Silva EA, Yuen WW, Mooney DJ. Spatio-temporal VEGF and PDGF delivery patterns blood vessel formation and maturation. *Pharmaceutical Research* 24, 258, 2007.
3. Dor Y, Djonov V, Keshet E. Making vascular networks in the adult: branching morphogenesis without a roadmap. *Trends in Cell Biology* 13, 131, 2003.
4. Ehrbar M, Djonov VG, Schnell C, Tschanz SA, Martiny-Baron G, Schenk U, Wood J, Burri PH, Hubbell JA, Zisch AH. *Circulation* 94, 1124, 2004.
5. Ferrara N, Gerber HP, LeCouter J. The biology of VEGF and its receptors. *Nature Medicine* 9, 669, 2003.
6. Glover DJ, Lipps HJ, Jans DA. Towards safe, non-viral therapeutic gene expression in humans. *Nature Reviews Genetics* 6, 299, 2005.
7. Heron M, Hoyert DL, Murphy SL, Xu J, Kochanek KD, Tejada-Vera B. Deaths: final data for 2006. *National Vital Statistics Report* 57, 1, 2009.
8. Hong K, Sherley J, Lauffenburger DA. Methylation of episomal plasmids as a barrier to transient gene expression via a synthetic delivery vector. *Biomolecular Engineering* 18, 185, 2001.
9. Jeong JH, Chan V, Cha C, Zorlutuna P, Dyck C, Hsia KJ, Bashir R, Kong H. “Living” microvascular stamp for patterning of functional neovessels; orchestrated control of matrix property and geometry. *Advanced Materials*, 2011.
10. Khademhoseini A, Vacanti JP, Langer R. Progress in tissue engineering. *Scientific American* 300, 64, 2009.
11. Khademhosseini A, Langer R, Borenstein J, Vacanti JP. Microscale technologies for tissue engineering and biology. *Proceedings of the National Academy of Sciences USA* 103, 2480, 2006.
12. Kong HJ, Kim ES, Huang YC, Mooney DJ. Design of biodegradable hydrogel for the local and sustained delivery of angiogenic plasmid DNA. *Pharmaceutical Research* 25, 1230, 2008.
13. Lei Y, Haider HK, Jiang SJ, Sim ESK. Therapeutic angiogenesis - devising new strategies based on past experiences. *Basic Research in Cardiology* 99, 121, 2004.

14. Levenberg S, Rouwkema J, Macdonald M, Garfein ES, Kohane DS, Darland DC, Marini R, van Blitterswijk CA, Mulligan RC, D'Amore PA, Langer R. Engineering vascularized skeletal muscle tissue. *Nature Biotechnology* 7, 879, 2005.
15. Raeber GP, Lutolf MP, Hubbell JA. Molecularly Engineered PEG Hydrogels: A Novel Model System for Proteolytically Mediated Cell Migration. *Biophysical Journal* 89, 1374, 2005.
16. Rouwkema J, Rivron NC, van Blitterswijk CA. Vascularization in tissue engineering. *Trends in Biotechnology* 26, 434, 2008.
17. Silva EA and Mooney DJ. Effects of VEGF temporal and spatial presentation on angiogenesis. *Biomaterials* 31, 1235, 2010.
18. Zisch AH, Lutolf MP, Hubbell JA. Biopolymeric delivery matrices for angiogenic growth factors. *Cardiovascular Pathology* 12, 295, 2003.

4.7 Figures

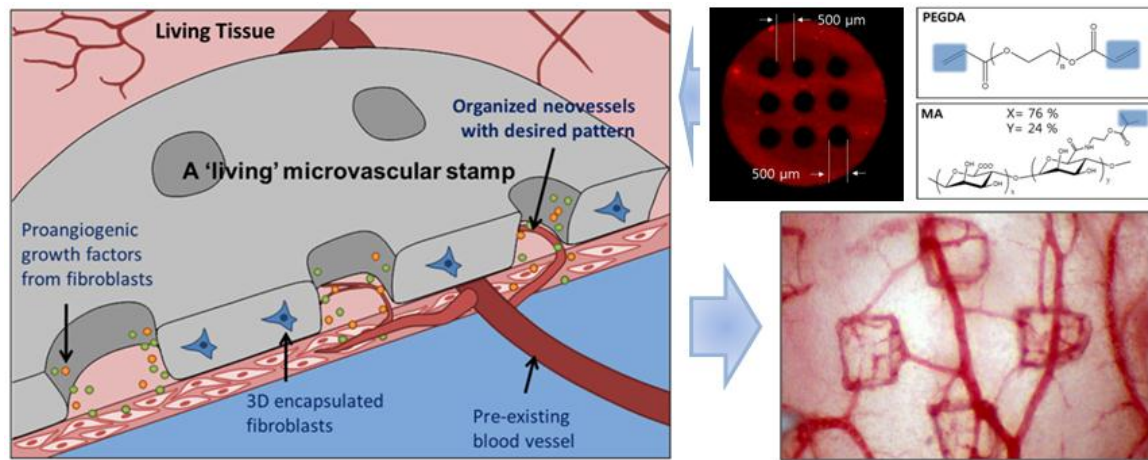


Figure 4.1 “Living” microvascular stamp for patterning of functional neovessels. The microvascular stamp incorporates cells in a hydrogel structure for patterned blood vessel formation (Jeong et al, 2011).

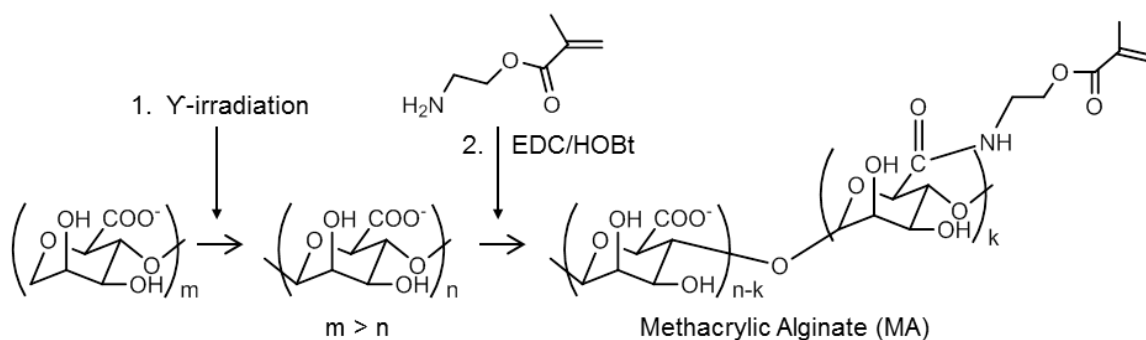


Figure 4.2 Synthesis of methacrylic alginate (MA). First, low molecular weight alginate was obtained by γ -irradiation of alginate rich in glucuronic acid residues. Aminoethylmethacrylate was then conjugated to the alginate molecules using carbodiimide chemistry.

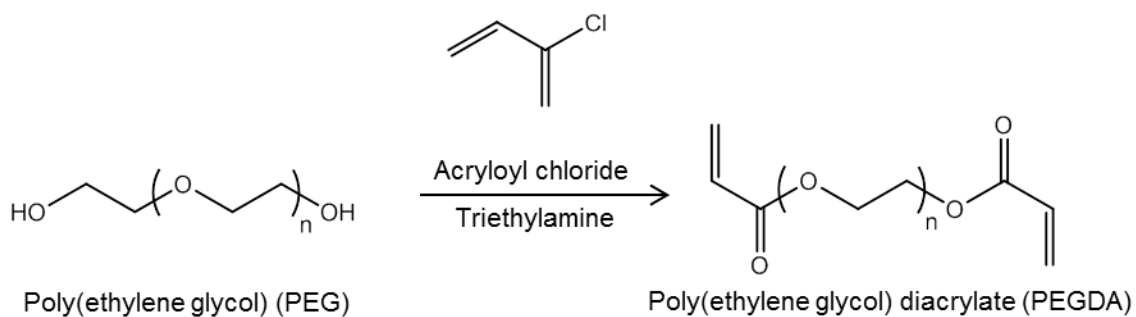


Figure 4.3 Synthesis of poly(ethylene glycol) diacrylate (PEGDA). Poly(ethylene) glycol (PEG) was reacted with acryloyl chloride and triethylamine to form PEGDA.

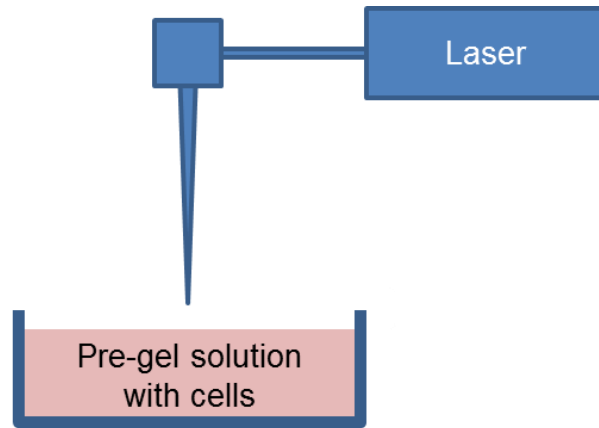


Figure 4.4 Stereolithography apparatus (SLA) for microvascular stamp fabrication. Cells were suspended in a pre-gel solution of PEGDA and methacrylic alginate (MA). The pre-gel solution was then polymerized using SLA.

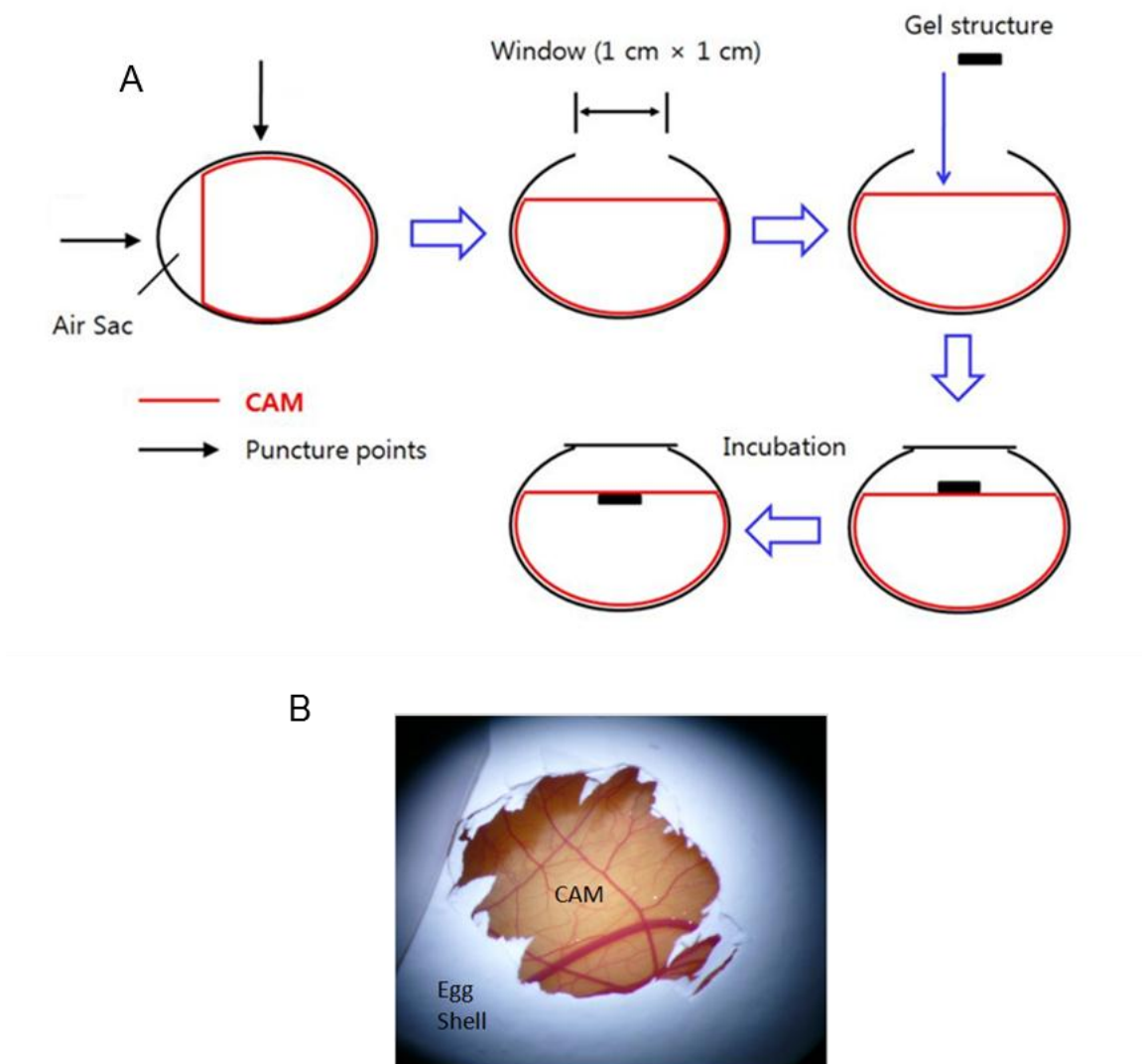


Figure 4.5 In-shell CAM angiogenesis assay. (A) Embryonic chicken eggs were incubated at 37 °C with 5 % CO₂. On the 9th day of gestation, a small window (1 × 1 cm) was created on top of each egg. After one day of additional incubation to stabilize the embryos, hydrogels were implanted on top of the CAM. Membranes were excised after seven days of incubation. (B) Photo of an in-shell CAM.

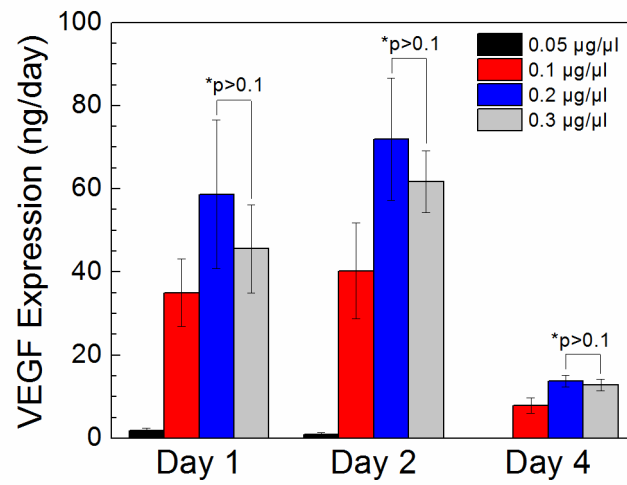


Figure 4.6 Effect of pDNA dose on VEGF expression. VEGF expression increased as the pDNA dose was increased from 0.05 µg/µl to 0.2 µg/µl but exhibited no statistically significant difference as the pDNA dose was increased further to 0.3 µg/µl (* $p > 0.1$). Values and error bars represent the mean and standard deviation from four independent measurements.

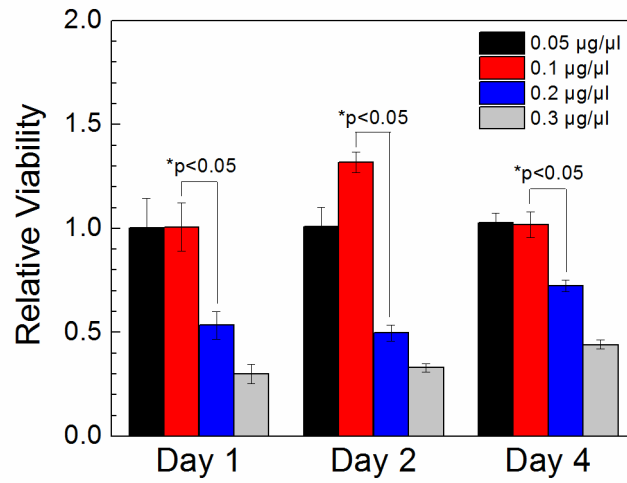


Figure 4.7 Effect of pDNA dose on cell viability. As the pDNA concentration was increased from 0.1 µg/µl to 0.2 µg/µl, the relative viability, which refers to the viability of transfected cells normalized with the viability of cells electroporated with 0 µg/µl pDNA, decreased. The differences between relative viability with 0.1 µg/µl and 0.2 µg/µl were statistically significant at all time points (* $p < 0.05$). Values and error bars represent the mean and standard deviation from four independent measurements.

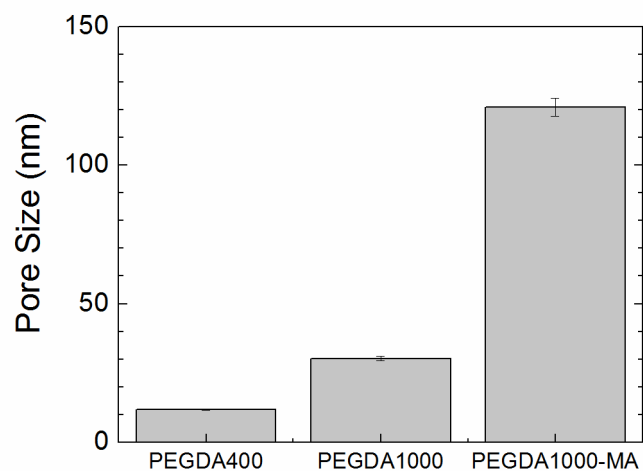


Figure 4.8 Hydrogel pore size. As the molecular weight of the PEGDA was increased from 400 to 1000 g/mol, the pore size of the hydrogel network increased. The addition of methacrylic alginate (MA) further increased the pore size in the hydrogel network. PEGDA400 and PEGDA1000 represent pure PEGDA hydrogels formed from PEGDA with molecular weights of 400 and 1000 g/mol, respectively. PEGDA1000-MA represents a hydrogel formed from PEGDA1000 and methacrylic alginate (MA). The total polymer concentration of all solutions was kept constant at 10% (w/v). Values and error bars represent the mean and standard deviation from four independent measurements.

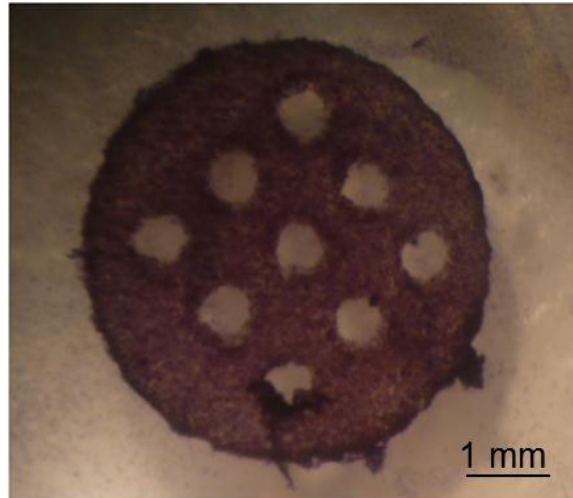


Figure 4.9 Cell viability following encapsulation in microvascular stamp. NIH3T3 fibroblasts transfected with pDNA encoding VEGF were incorporated in microvascular stamps using a stereolithography apparatus (SLA). The cells remained viable after encapsulation, as evidenced by the dark stain following treatment with an MTT reagent.

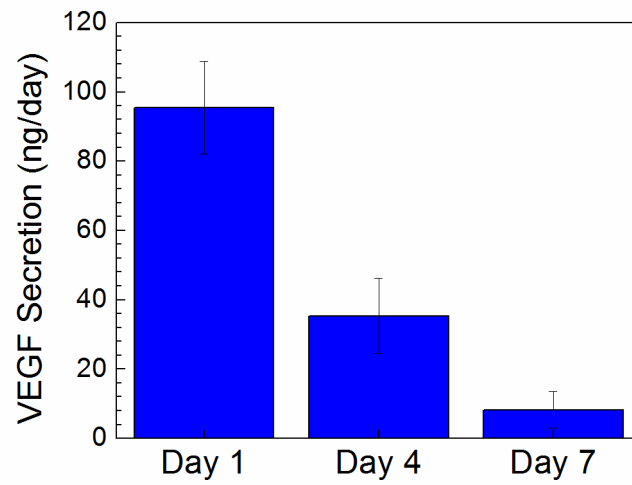


Figure 4.10 VEGF secretion from microvascular stamps. NIH3T3 fibroblasts transfected with pDNA encoding VEGF were incorporated in microvascular stamps. The amount of VEGF secreted from the microvascular stamps decreased over 7 days. Values and error bars represent the mean and standard deviation from four independent measurements.

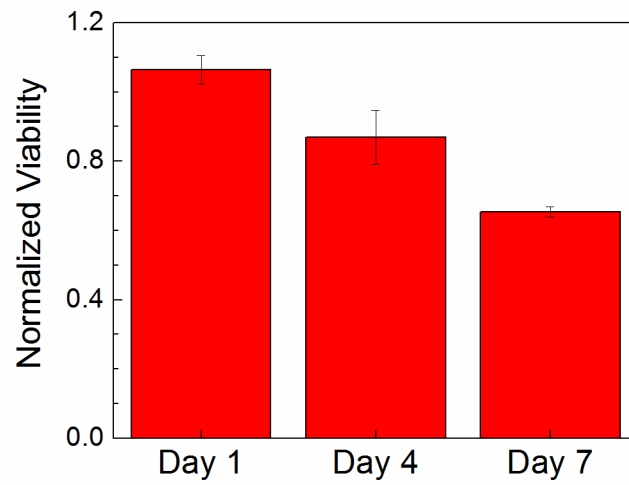


Figure 4.11 Cell viability in microvascular stamps. NIH3T3 fibroblasts transfected with pDNA encoding VEGF were incorporated in microvascular stamps. The cell viability was measured on Days 1, 4, and 7, and the values were normalized to the cell viability measured 4 hours after encapsulation. Values and error bars represent the mean and standard deviation from four independent measurements.

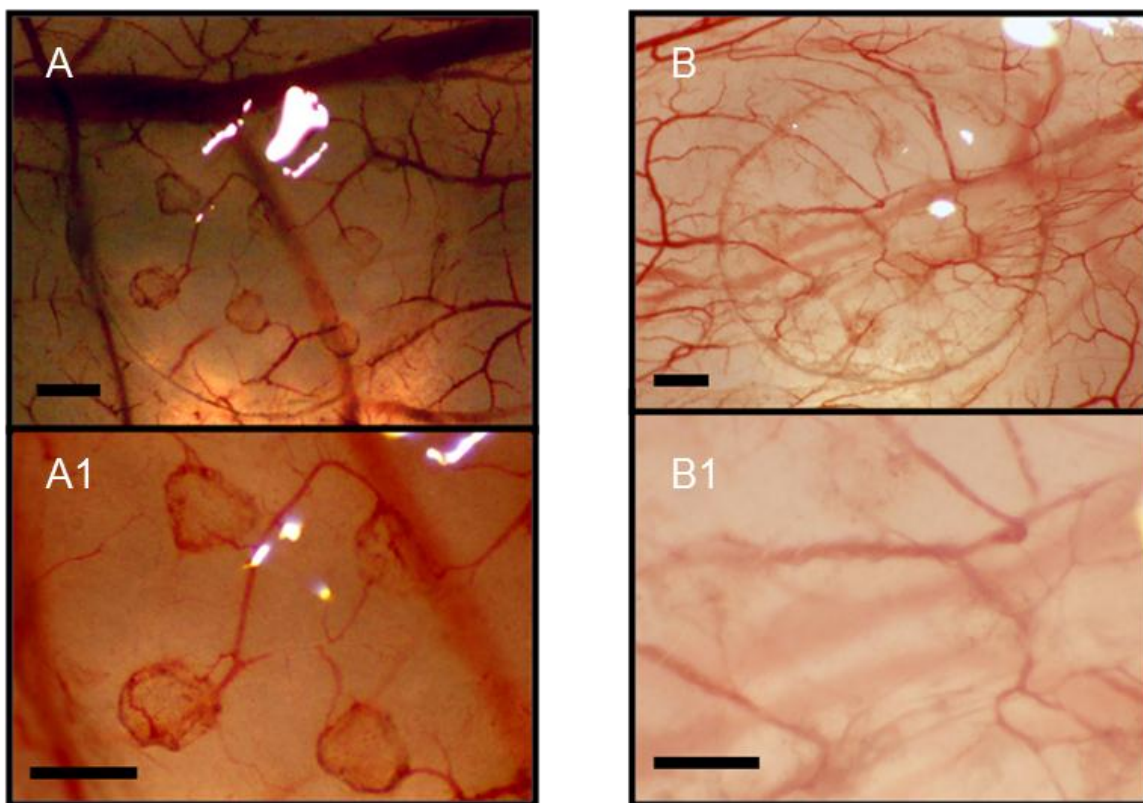


Figure 4.12 Blood vessel formation from microvascular stamps. (A) Neovessels formed along microchannels in the microvascular stamp fabricated with cells that had been transfected with pDNA encoding VEGF. (B) Microvascular stamp fabricated with cells that were not manipulated to secrete VEGF. Images in A and B were further magnified in A1 and B1, respectively. Scale bars represent 500 μm .



Figure 4.13 Inflammatory response from microvascular stamp with high cell density. With an increased density of cells transfected with pDNA encoding VEGF (5×10^6 cells/ml), microvascular stamps elicited a pro-inflammatory response on the CAM, characterized by the formation of fibrous tissue on the surface of the vascular stamp. Scale bar represents 500 μm .